

# A 700-year rupture sequence of great eastern Aleutian earthquakes from tsunami modeling of stratigraphic records

Received: 9 July 2024

Accepted: 4 March 2025

Published online: 17 March 2025

 Check for updatesYoshiki Yamazaki<sup>1</sup>, Kwok Fai Cheung<sup>1</sup>✉, Thorne Lay<sup>2</sup>, SeanPaul M. La Selle<sup>3</sup>, Robert C. Witter<sup>4</sup> & Bruce E. Jaffe<sup>3</sup>

Great Aleutian underthrusting earthquakes produced destructive tsunamis impacting Hawai'i in 1946 and 1957. Prior modeling of the 1957 tsunami deposit and runup records on eastern Aleutian and Hawaiian Islands jointly with tide-gauge observations across the Pacific Ocean constrained a rupture model with shallow slip up to 26 m along 600 km of the plate boundary. Here we implement this modeling approach to older deposits and show alternating deep and shallow megathrust slip up to 26, 32, and 22 m for great earthquakes along the same segment in the 18<sup>th</sup>, 15<sup>th</sup>, and 14<sup>th</sup> centuries. All three modeled prehistoric Aleutian earthquakes produce tsunami inundation in Hawai'i with the most severe, 14<sup>th</sup> century event having impacts exceeding the 1957 event. The along-dip variability of these four ruptures spanning seven centuries provides insights on earthquake cycles for engineering design and hazard assessment. The 15<sup>th</sup> century and 1957 rupture models provide evidence for recurrence of tsunami earthquakes, which can produce disproportionately large tsunamis for a given moment magnitude due to reduced rigidity in the shallow megathrust. The 14<sup>th</sup> and 18<sup>th</sup> century events likely ruptured deeper regions that did not slip in 1957, suggesting potential for corresponding deeper failure in the next great eastern Aleutian earthquake.

The Hawaiian Islands in the central North Pacific Ocean are exposed to multiple sources of tsunamis generated by subduction zone earthquakes around the Pacific margin. Assessing the tsunami hazard requires information about the distribution and recurrence of great earthquakes, but the historical record is short and varies from region to region. The nearest and most critical subduction zone to Hawai'i lies to the north along the Aleutian Islands (Fig. 1a), where the Pacific plate underthrusts the North America plate at a rate of 6.6–7.4 cm/yr<sup>1</sup>. This region hosted several great earthquakes during the last century, including the 1946  $M_W$  8.6 Aleutian Islands, 1957  $M_W$  8.6–8.8 Aleutian Islands, and 1965  $M_W$  8.7 Rat Islands events<sup>2–4</sup>, all of which generated destructive tsunamis with observed runup exceeding 10 m near the source<sup>5</sup>, but varying impacts across the Pacific Ocean due to wave directionality.

Great underthrusting events produce strong trench-perpendicular tsunami radiation, which combined with curvature of the Aleutian Arc, makes the eastern 600 km of the 1200-km long 1957 rupture zone and the adjacent 200-km long 1946 rupture zone a primary tsunami threat for Hawai'i<sup>6</sup>. Recent geodetic surveys along this stretch of subduction zone have shed some light on the complex interplate movement and strain accumulation. The measurements suggest current creeping of the deeper plate boundary along Unimak and Unalaska Islands and moderate slip deficit accumulation along Umnak Island (Fig. 1a), but are unable to resolve shallow slip deficit due to block rotation and lateral translation in the upper plate as well as the large distance from the stations to the trench<sup>7–9</sup>. Because of the lack of information on the potentially most tsunamigenic shallow plate

<sup>1</sup>Department of Ocean and Resources Engineering, University of Hawai'i at Manoa, Honolulu, HI, USA. <sup>2</sup>Department of Earth and Planetary Sciences, University of California Santa Cruz, Santa Cruz, CA, USA. <sup>3</sup>U.S. Geological Survey, Pacific Coastal and Marine Science Center, Santa Cruz, CA, USA. <sup>4</sup>U.S. Geological Survey, Alaska Science Center, Anchorage, AK, USA. ✉e-mail: [cheung@hawaii.edu](mailto:cheung@hawaii.edu)

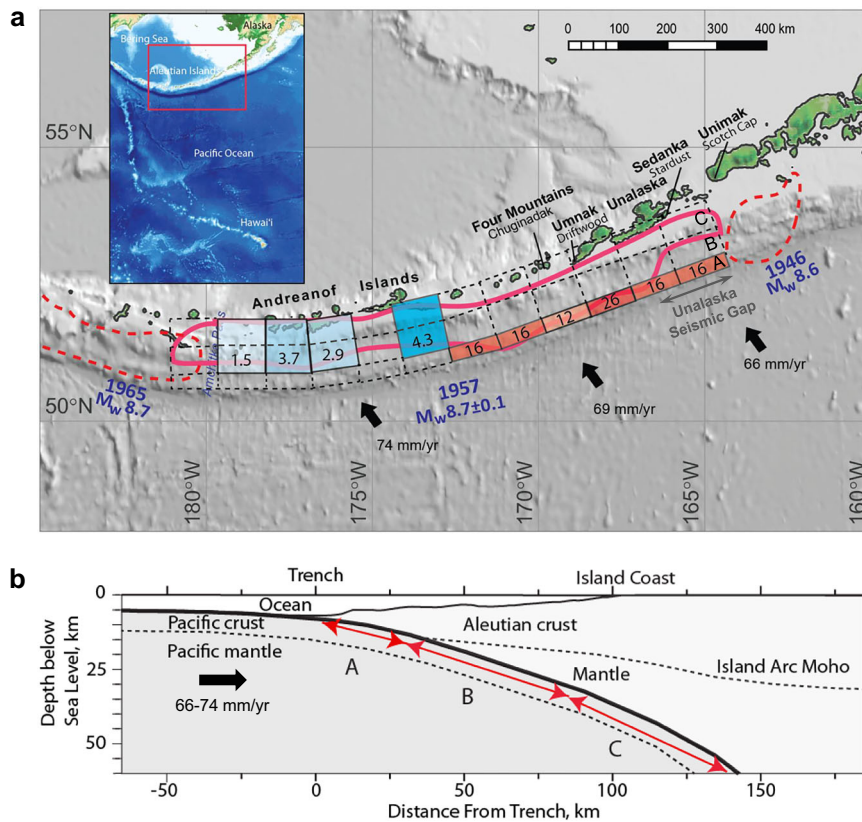


**Fig. 1 | Great earthquakes and rupture grid at the Aleutian Arc. a** Great earthquakes in the 20<sup>th</sup> century. Inset numbers over the 3 by 12 grid indicate subfaults with large slip in meters from the updated 1957 rupture model<sup>3</sup> with red and blue tones for shallow and deeper megathrust rupture, respectively. Red solid and dashed lines indicate relocated aftershock zones of the 1957 Aleutian Islands earthquake, the 1946 Aleutian Islands tsunami earthquake, and the 1965 Rat Islands earthquake<sup>4</sup>. Arrows and labels indicate Pacific plate convergence direction and rate relative to a fixed North American/Bering Sea plate from the MORVEL model<sup>1</sup>.

The approximate extent of the proposed Unalaska gap<sup>2,30</sup> in the shallow megathrust is indicated in gray. The inset map shows the Hawaiian Islands in relation to the Aleutian tsunami source region. Base maps generated from [https://www.gebco.net/data\\_and\\_products/gridded\\_bathymetry\\_data/](https://www.gebco.net/data_and_products/gridded_bathymetry_data/). **b** Schematic cross section. The near-trench, central, and down-dip regions across the plate boundary are classified as Domains A, B, and C<sup>10</sup>, which are represented by the three along-strike rows of subfaults to account for depth-dependent rupture and tsunamigenic properties.

boundary, assessment of tsunami hazards currently depends on historical records and prehistoric geologic evidence of great earthquakes in the region.

Rupture properties of megathrust earthquakes vary with depth across the plate boundary (Fig. 1b). The near-trench, central, and down-dip regions, which are classified as Domains A, B, and C, tend to host tsunami, large-slip, and moderate-slip earthquakes<sup>10</sup>. In the eastern Aleutian subduction zone, Domain A spans the upper plate crust and slab contact down to about 15 km depth<sup>11</sup>, whereas Domains B and C are along the upper plate mantle and slab interface. Seismic imaging has detected low P velocities in the upper plate outer forearc along Domain A, whereas much higher velocities exist along the mantle and slab interface for deeper Domains B and C<sup>12</sup>. The low P velocities reflect reduced, shallow megathrust rigidity that results in longer source process time and less short-period ground shaking recorded by instruments. As a result, the moment magnitude can be disproportionately small compared to the tsunami generated by a given fault slip. The 1946 rupture was such a tsunami earthquake<sup>13–15</sup> that involved large, relatively slow slip along the shallow plate boundary<sup>16,17</sup>. The attendant tsunami produced up to 42 m runup at Scotch Cap, Unimak Island<sup>18</sup>, and the most destructive event documented in Hawai'i<sup>19</sup>. The rupture zone is located in a region for which recent geodetic slip deficit is not detected<sup>20</sup>.

Both near and far-field tsunamis vary notably with the source water depth across the continental margin<sup>21,22</sup>, providing important linkage to depth-dependent rupture properties. The 1957 tsunami

deposited sand and drift logs at 12–32 m elevation above present mean sea level on multiple eastern Aleutian Islands<sup>23–25</sup>, which together with a local tide gauge record, can only be explained by large nearby shallow slip<sup>26</sup> not resolved in earlier modeling<sup>27,28</sup>. The 1957 tsunami also left behind sandy deposits<sup>29</sup> and produced large observed runup reaching 16.2 m in the Hawaiian Islands, close to the 16.4 m peak runup for the 1946 event<sup>19</sup>. With a subfault grid accounting for depth dependent rupture and tsunamigenic properties from Domains A through C, an updated 1957 fault-slip model<sup>3</sup> is able to resolve considerable shallow slip up to 26 m in the eastern 600 km of the rupture zone as well as moderate, deeper slip in the western half of the rupture (Fig. 1a). The slip distribution can account for tsunami deposit and runup records along the eastern Aleutian and Hawaiian Islands, tide gauge records across the Pacific Ocean as well as an on-scale long-period seismic recording<sup>28</sup> and -95% of the length of the relocated aftershock region<sup>4</sup> along strike. The well-constrained large slip in the easternmost rupture zone substantiates prior work<sup>23,24,26</sup> in negating the Unalaska seismic gap<sup>2,30</sup>, which was proposed by the lack of 1957 shallow aftershocks off Unalaska Island and the absence of eastern shallow slip in earlier rupture models<sup>27,28</sup>. The eastern 600-km long shallow rupture constitutes an  $M_w$  8.3–8.6 tsunami earthquake component of the 1957  $M_w$  8.6–8.8 rupture<sup>3</sup>, resulting in tsunami impacts on Hawai'i that were comparable to those produced by the 1946 earthquake.

Here we show stratigraphic records from two eastern Aleutian Islands and three Hawaiian Islands<sup>23,24,29</sup> used to constrain the updated 1957 rupture model<sup>3</sup> also include deposits from three prior large

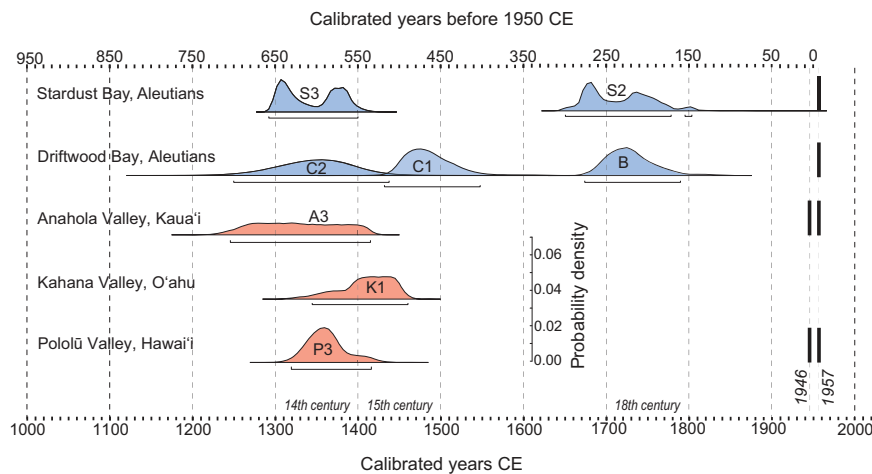


**Fig. 2 | Compiled chronology of prehistoric and historical tsunami events.** Probability density distributions represent calibrated radiocarbon dates of tsunami deposits at eastern Aleutian and Hawai'i sites in the 14<sup>th</sup>, 15<sup>th</sup>, and 18<sup>th</sup> centuries. Bars beneath distributions show 95% confidence intervals. Labels above distributions,

such as S2 and S3, identify distinct sand layers found at multiple core locations at each site<sup>23,24,29</sup>. Vertical bars indicate presence of tsunami deposits from the 1946 and 1957 events.

tsunamis for inference of great Aleutian earthquakes in the last 700 years. The earliest is a 14<sup>th</sup> century event that likely produced deposits at all five sites, while events in the 15<sup>th</sup> and 18<sup>th</sup> centuries produced deposits at one and both Aleutian sites, respectively (Fig. 2). With a deposit layer (K1) saddling between the 14<sup>th</sup> and 15<sup>th</sup> centuries, the records suggest only one or two tsunami deposits in Hawai'i in the six centuries before the 1946 event, and this is surprising given the experiences of five destructive tsunamis during the 20<sup>th</sup> century<sup>19</sup>. Despite the uncertainties, the near and far-field geologic observations, as well as their absence at specific sites, provide constraints in delineating plate boundary slip along dip and strike for the prehistoric events. Following the protocol used for the updated 1957 rupture modeling<sup>3</sup>, we reconstruct slip distributions for the 14<sup>th</sup>, 15<sup>th</sup>, and 18<sup>th</sup> century earthquakes that reproduce paleo-tsunami inundation inferred from the stratigraphic records<sup>23,24,29</sup>. The modeling links stratigraphic records thousands of kilometers apart and examines whether all three large Aleutian tsunamis produced inundation in Hawai'i despite absence of deposits for some of the events. The results, together with the updated 1957 rupture model<sup>3</sup>, provide a 700-year sequence of great earthquakes that contributes to understanding one of the most seismically active plate boundaries in the world and the knowledge base for assessment of tsunami hazard exposure in the north central Pacific region.

## Results

Tsunami computation with the nonhydrostatic model NEOWAVE<sup>31,32</sup> covers a wide parameter space of slip placement over the 150 km by 600 km plate interface in the eastern half of the 1957 rupture zone (Fig. 1a). The modeling involved 34, 17, and 69 iterations of the slip distributions over the 3 × 6 subfault grid for the 18<sup>th</sup>, 15<sup>th</sup>, and 14<sup>th</sup> century ruptures, respectively. Selection of the preferred model for each event is based on a number of criteria. First of all, we seek simple slip distributions with the lowest seismic moment that can account for the inundation inferred from paleotsunami deposits, and for which slip is confined to a minimum number of subfaults. Issues with tsunami deposit preservation may introduce uncertainty into the comparison between computed inundation and locations of sandy deposits. The recent modeling of the 1957 event<sup>3</sup> corroborates a 1-m flow depth<sup>33</sup> as the threshold to produce detectable sediment deposits at the Aleutian sites, where the sediment supply is abundant and deposits are relatively well preserved, but suggests a higher threshold of ~3 m in the tropical wetland environments of Hawai'i. The higher threshold might

be due to the core locations in alluvial plains subject to freshwater runoff and channel overflow during the wet season. Tropical island reefs, in some cases, may limit the supply of sandy sediment transported inland by tsunamis<sup>34</sup>. The interseismic accumulation of slip deficit from the current plate convergence of 7 cm/yr along the eastern Aleutian Islands<sup>1</sup> provides an additional constraint in selecting preferred models for the sequence of ruptures over the last 700 years (see Methods for details). As such, the events are analyzed and presented in reverse chronological order to utilize information from the updated 1957 rupture model<sup>3</sup>.

### The 18<sup>th</sup> century event

Each of the three prehistoric events has distinct stratigraphic records for inference of potential tsunami wave patterns across the ocean and slip distributions over the 3 × 6 subfault grid. The 18<sup>th</sup> century event produced tsunami deposits reaching 23.0 m elevation above present mean sea level in the eastern Aleutian Islands, but none in Hawai'i directly due south (Fig. 1a). The use of NEOWAVE<sup>31,32</sup> is instrumental to describe higher-order, nonhydrostatic processes in water-depth dependent tsunami excitation on the continental slope as well as the rapidly attenuating wave field across the ocean as implied by the records (See Methods). Figures 3 and 4 show the preferred rupture model in Domain B as well as an alternate Domain A model together with the respective near and far-field tsunami wave amplitudes and comparisons of computed inundation and stratigraphic records at the two Aleutian and three Hawai'i sites.

The preferred rupture model has 26 m slip over a 60 km by 100 km Domain B subfault (Fig. 3a), down-dip of where the largest 26-m slip occurred in 1957 (Fig. 1a). Assuming a rigidity of 30 GPa for the central megathrust region, the seismic moment is estimated as  $M_0 = 4.68 \times 10^{21}$  Nm ( $M_W$  8.38). In nearby Driftwood Bay, the absence of deposits at cores above 23.0 m elevation provides a strong constraint on the computed runup. The central slip placement beneath shallower water reduces attenuation of the seafloor excitation to the sea surface and decrease refraction of the radiated waves toward the shore in maintaining sufficient wave amplitude at Stardust Bay 190 km to the northeast, which has at least 14.4 m runup inferred from the deposits reaching the uppermost cores (Fig. 3b, Supplementary Movie 1). Despite the relatively large subfault compared to typical finite fault models<sup>21</sup>, the computed tsunami inundation compares well with the deposit patterns and the 1-m flow depth contour is close to the uppermost deposits at both Aleutian sites (Fig. 3c).

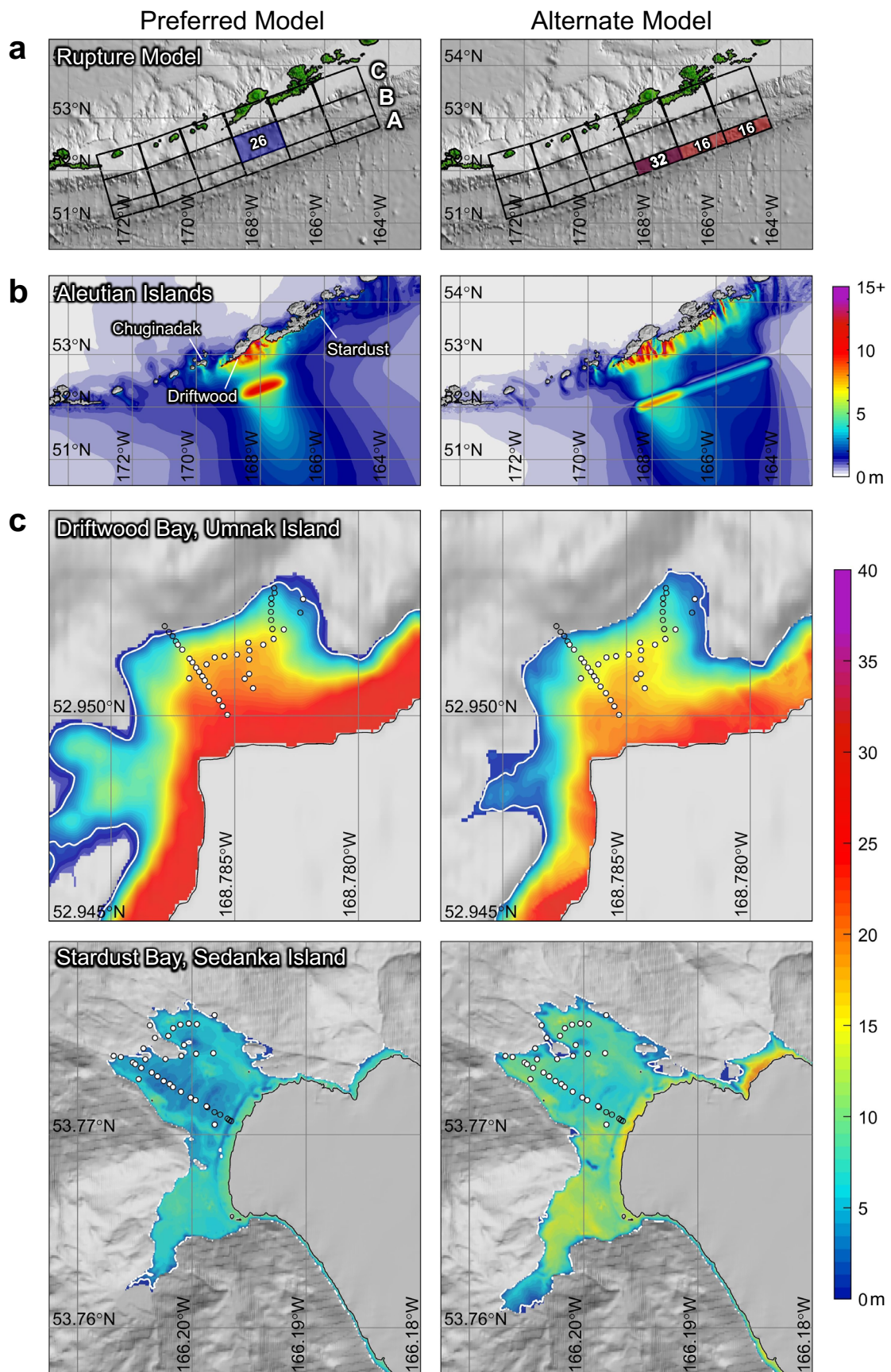


**Fig. 3 | Models for the 18<sup>th</sup> century rupture and near-field tsunami. a** Rupture model. Red and blue tones denote shallow and deeper megathrust slip in meters. **b** Near-field tsunami amplitude. **c** Computed flow depth and stratigraphic records at Aleutian sites. Base maps generated from <https://www.ncei.noaa.gov/maps/>

[bathymetry](https://www.ncei.noaa.gov/maps/). Black lines denote waterlines at present local mean sea level and white lines denote 1-m flow depth. Solid white and open circles mark the location of cores with and without coeval tsunami deposits (Source data available from <https://doi.org/10.5066/P9D7KLVJ>).

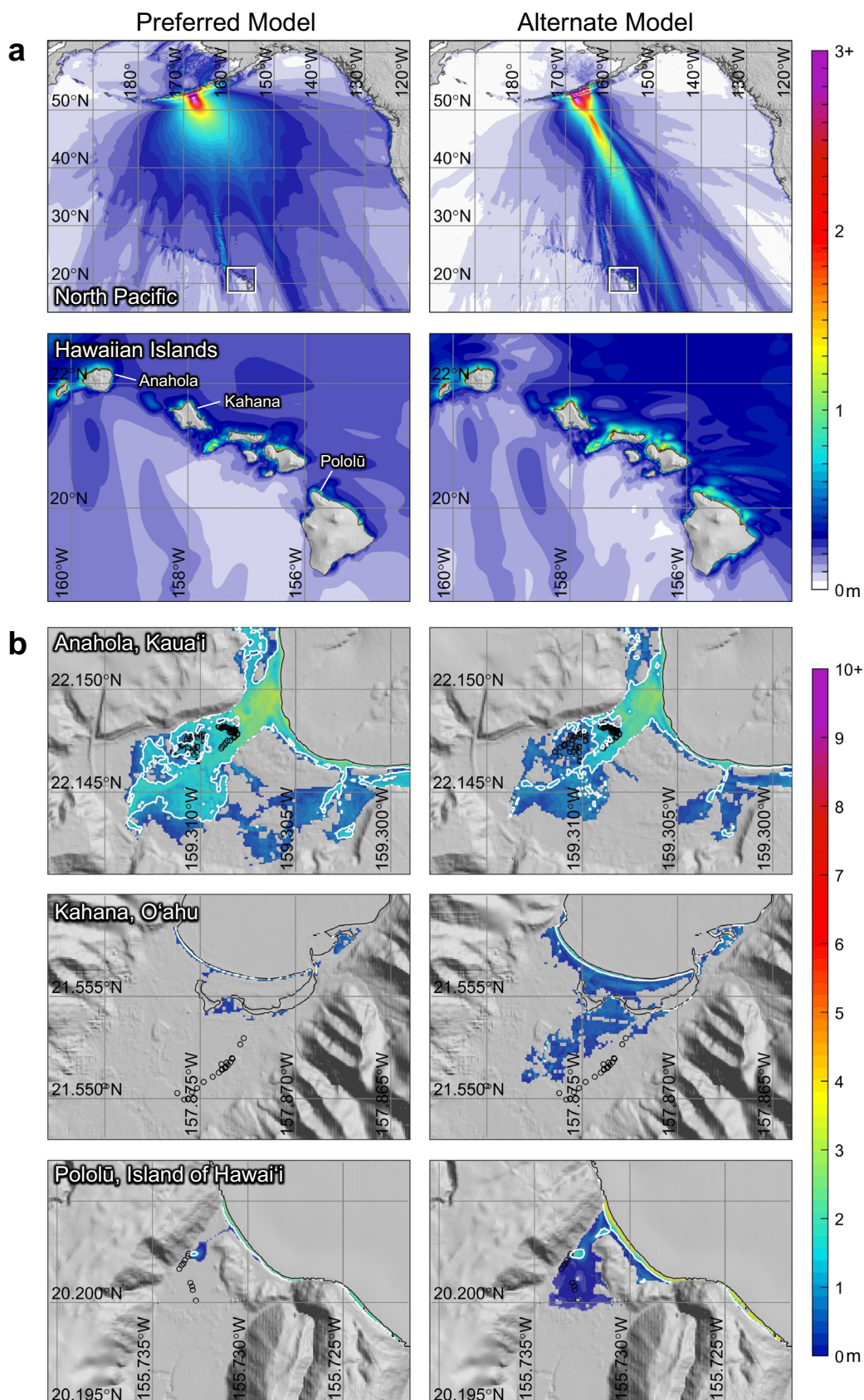


**Fig. 4 | Models for the 18<sup>th</sup> century far-field tsunami. a** Tsunami wave amplitude. White rectangles in upper panels delineate the Hawaiʻi region with higher resolution results shown in lower panels. **b** Computed flow depth and stratigraphic records at Hawaiʻi sites. Base maps generated from [https://www.gebco.net/data\\_and\\_products/gridded\\_bathymetry\\_data/](https://www.gebco.net/data_and_products/gridded_bathymetry_data/) and <https://www.ncei.noaa.gov/maps/bathymetry/>. Black lines denote waterlines at adjusted local mean sea level according to Table 1 and white lines denote 1-m flow depth. Solid white and open circles mark the location of cores with and without coeval tsunami deposits (Source data available from <https://doi.org/10.5066/P9X4STJM>).

The seaward tsunami attenuates rapidly due to radiation from a concentrated source over a large azimuth, de-shoaling from the upper continental slope, and dispersion of the short-period waves across the ocean (Fig. 4a). The waters around Hawai'i are prone to multi-scale resonance oscillations over a wide period range due to the varying size and proximity of the islands as well as the interconnected reef, shelf, and slope complexes<sup>35</sup>. The tsunami waves decrease to 0.2–0.25 m amplitude north of the islands, but trigger short-period oscillation modes over the insular shelves, which produce considerable inundation with flow depths reaching 1 and 2 m at the core locations in Pololū and Anahola Valleys, respectively (Fig. 4b). The short-period waves do not inundate Kahana Valley fronted by a relatively wide shelf with longer-period oscillation modes<sup>35</sup>. Assuming a flow depth threshold of 3 m to produce preservable deposits in this setting<sup>3</sup>, the computed inundation is consistent with absence of observed 18<sup>th</sup> century deposits in Hawai'i, supporting the rupture model constrained by stratigraphic records at the two Aleutian sites.

The alternate model, which involves shallow slip of 16–32 m in three Domain A subfaults of 30 km wide and 300 km long together, is notably different from the preferred, concentrated Domain B rupture in terms of depth, dimensions, and seismic moment (Fig. 3a). Despite the contrasting near and far-field wave patterns to those from the preferred model (Figs. 3b and 4a), the computed tsunami inundation matches equally well with the Aleutian deposits while maintaining less than 2-m flow depth at the core locations in Hawai'i consistent with the absence of deposits (Figs. 3c and 4b). The comparison of computed inundation patterns with the stratigraphic records alone cannot confidently distinguish between the two rupture models, highlighting the uncertainty and challenge in deducing paleo-tsunami sources. However, the large shallow slip in the alternate model indicates substantial strain release in the 18<sup>th</sup> century. An elapsed time of 200 years at the current convergent rate of 7 cm/yr<sup>1</sup> cannot provide enough accumulated strain for a repeated failure with 26 m slip in the 1957 earthquake (Fig. 1a), supporting the choice of the Domain B rupture as the preferred model.

### The 15<sup>th</sup> century event

The 15<sup>th</sup> century event produced tsunami deposits at 23.0 m elevation in Driftwood Bay, but no sedimentary evidence at Stardust Bay 190 km to the northeast (Fig. 2). The absence of deposits at cores above 23.0 m elevation provides a good constraint for the computed runup at the Driftwood Bay site. This pattern is best described by a tsunami earthquake with 32 m shallow slip in a 30 km by 100 km Domain A subfault fronting Umnak Island (Fig. 5a). Although there have been a number of proposed mechanisms for tsunami earthquakes<sup>36–38</sup>, most recent historical events can be explained by reduced rigidity in the shallow megathrust<sup>39</sup>. Assuming a low rigidity of 10 GPa for the shallow megathrust, the seismic moment is estimated as  $M_0 = 9.60 \times 10^{20}$  Nm ( $M_W$  7.92). The excitation from a narrow slip patch beneath deeper water near the trench attenuates over the water column yielding initial wave amplitude notably smaller than the seafloor vertical displacement<sup>32</sup>. The resulting tsunami has dominant short-period components that more effectively shoal on the continental slope and refract across the shelf edge to modulate the alongshore wave amplitude (Fig. 5b). The amplified and focused waves result in severe inundation matching the stratigraphic records in Driftwood Bay immediately shoreward but produce only minor inundation with flow depth less than the 1-m threshold<sup>33</sup> at all but one core in the adjacent Stardust Bay (Fig. 5c, Supplementary Movie 2).

The short period tsunami waves attenuate rapidly across the ocean due to dispersion and produce minor oscillations over the insular shelves along the Hawaiian Islands (Fig. 6a). Sedimentary evidence of this event was not found at Anahola and Pololū, while the age uncertainty of the deposit in Kahana Valley can neither confirm nor rule out a 15<sup>th</sup> century Aleutian tsunami source (Fig. 2). The computed tsunami inundation has less than 1 m flow depth at the core locations in

Anahola Bay consistent with the absence of sedimentary evidence and is limited to the foreshore areas far from the cores at the Kahana and Pololū sites (Fig. 6b). Kahana Valley was probably not severely impacted by the 15<sup>th</sup> century tsunami with predominantly short period waves as suggested by the modeling; the paleotsunami deposit is more likely from the earlier 14<sup>th</sup> century event. Given the considerable distance between the core locations and the shoreline and the high flow-depth threshold of ~3 m for preservable deposits<sup>3</sup>, a wide range of inundation can be inferred from the absence of deposits at the Hawai'i sites. The primary constraints on the rupture model are the stratigraphic records in Driftwood and Stardust Bays for this event.

The active near-trench segment inferred for the 15<sup>th</sup> century event was re-ruptured with 26 m slip in the 1957 earthquake<sup>3</sup>. Given the current convergent rate of 7 cm/year, the amount of slip involved is within the maximum possible deficit of 35 m in 500 years, indicating strong coupling of the shallow interface not detected by recent geodetic surveys<sup>7–9</sup>. The alternate model has 32 m slip in a Domain B subfault constrained by tsunami runup inferred from the deposits in Driftwood Bay (Fig. 5a, c). The large initial wave over the upper continental slope does not attenuate sufficiently along the margin (Fig. 5b). The computed inundation extends to most of the cores with sufficient flow depths for sediment preservation at the Stardust Bay site (Fig. 5c), contrary to the absence of deposits in the stratigraphic records. This significant mismatch between the computed and inferred inundation is sufficient to negate the Domain B rupture model, even though the wave amplitude attenuates sufficiently across the North Pacific and the inundation at the Hawai'i sites is still within the range that can be explained by the absence of deposits (Fig. 6). The alternate model is also an unlikely candidate due to re-rupture of the same segment in the preferred 18<sup>th</sup> century model.

### The 14<sup>th</sup> century event

The 14<sup>th</sup> century tsunami likely produced sediment deposits at all Aleutian and Hawai'i sites. The preferred rupture spans the six Domain B subfaults over an area of 60 km by 600 km across the model grid; the slip increases from 7 to 22 m eastward to reconcile the overall fit to the stratigraphic records (Fig. 7a). A rigidity of 30 GPa yields a seismic moment of  $M_0 = 1.3 \times 10^{22}$  Nm ( $M_W$  8.68). The elongated rupture zone beneath the upper continental slope produces a long-crested initial wave with increased amplitude and period on the east side (Fig. 7b). The 13.3 m runup inferred at the Driftwood Bay site is well constrained by absence of sand deposits at higher-elevation cores and is well matched by the 7 m slip immediately offshore (Fig. 7c). The slip westward is not constrained by local stratigraphic records, but is needed to produce ~4 m tsunami amplitude off Chuginadak Island (Fig. 7b) and to increase the tsunami energy directed toward Hawai'i. The 15<sup>th</sup> and 18<sup>th</sup> century models also produce ~4 m wave amplitude off Chuginadak Island (Figs. 3b and 5b), which may explain the provenance of undated deposits<sup>25</sup> beneath the 1957 layer at elevations as high as 9 m. At the Stardust Bay site, sedimentation extends to the uppermost core at 14.3 m elevation, which represents a lower bound estimate of the runup (Fig. 7c). The 22 m eastern slip, which produces inundation inland of the cores, is constrained by the stratigraphic records in Hawai'i.

Among the three prehistoric events, the 14<sup>th</sup> century tsunami produces the most severe impact at the Hawai'i sites exceeding the computed 1957 inundation<sup>3</sup>. The initial pulse spanning 600 km of the eastern Aleutian arc produces a main lobe that is more focused across the North Pacific Ocean than the other two prehistoric events (Fig. 8a, Supplementary Movie 3). The broad-band tsunami waves trigger both island-scale and inter-island oscillation modes<sup>35</sup> with amplified waves beyond the insular shelves and slopes along the Hawaiian Islands. The modeled tsunami inundates the entire alluvial plain of Anahola Valley with ~3 m flow depth at the cores with deposits and produces ~2 m flow depth at the deposit in Pololū Valley (Fig. 8b). The latter is below the threshold, but is given lesser weight in deducing the rupture model,

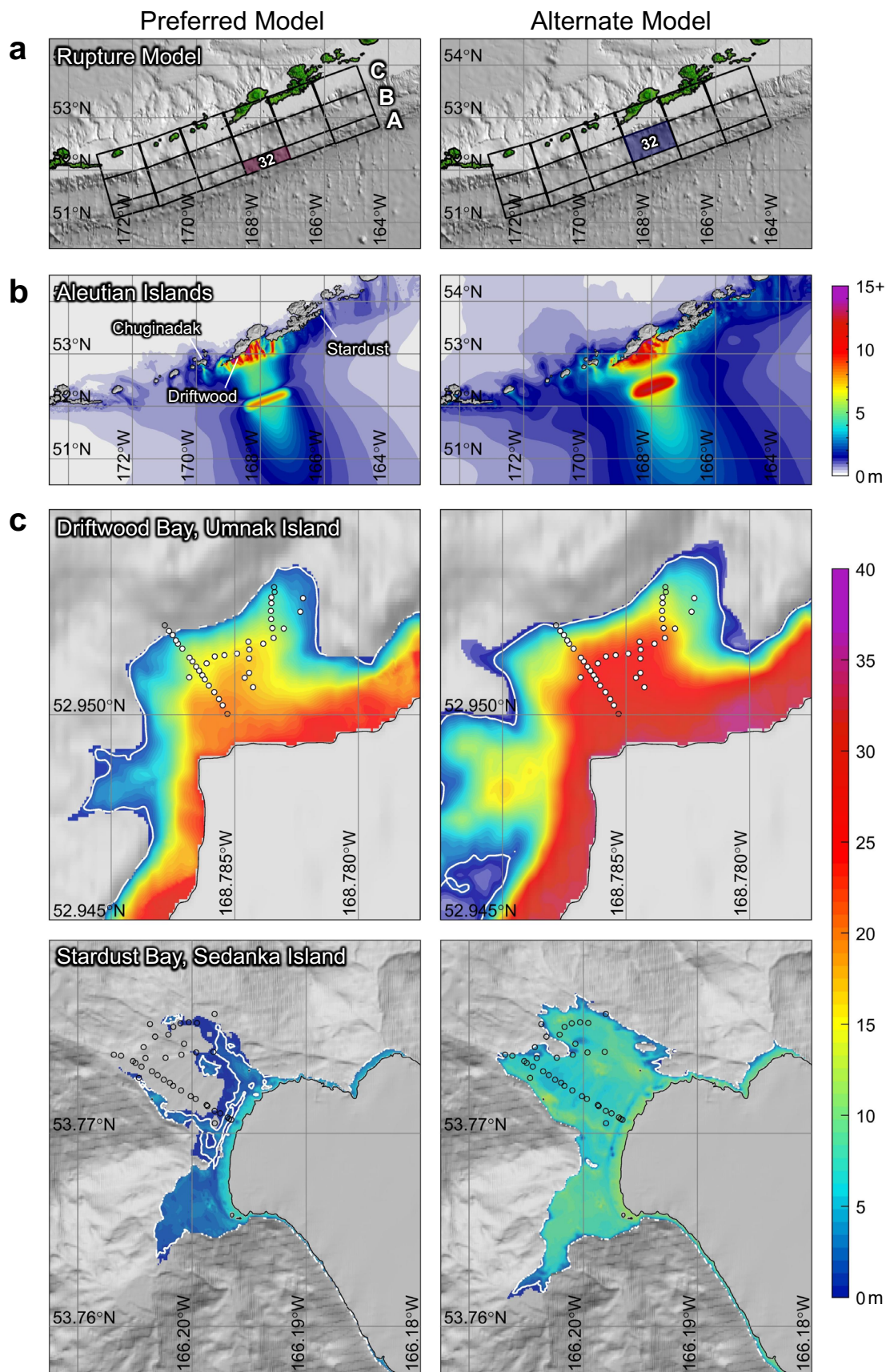


**Fig. 5 | Models for the 15<sup>th</sup> century rupture and near-field tsunami. a** Rupture model. Red and blue tones denote shallow and deeper megathrust slip in meters. **b** Near-field tsunami amplitude. **c** Computed flow depth and stratigraphic records at Aleutian sites. Base maps generated from <https://www.ncei.noaa.gov/maps/>

[bathymetry/](https://www.ncei.noaa.gov/maps/). Black lines denote waterlines at present local mean sea level and white lines denote 1-m flow depth. Solid white and open circles mark the location of cores with and without coeval tsunami deposits (Source data available from <https://doi.org/10.5066/P9D7KLVJ>).

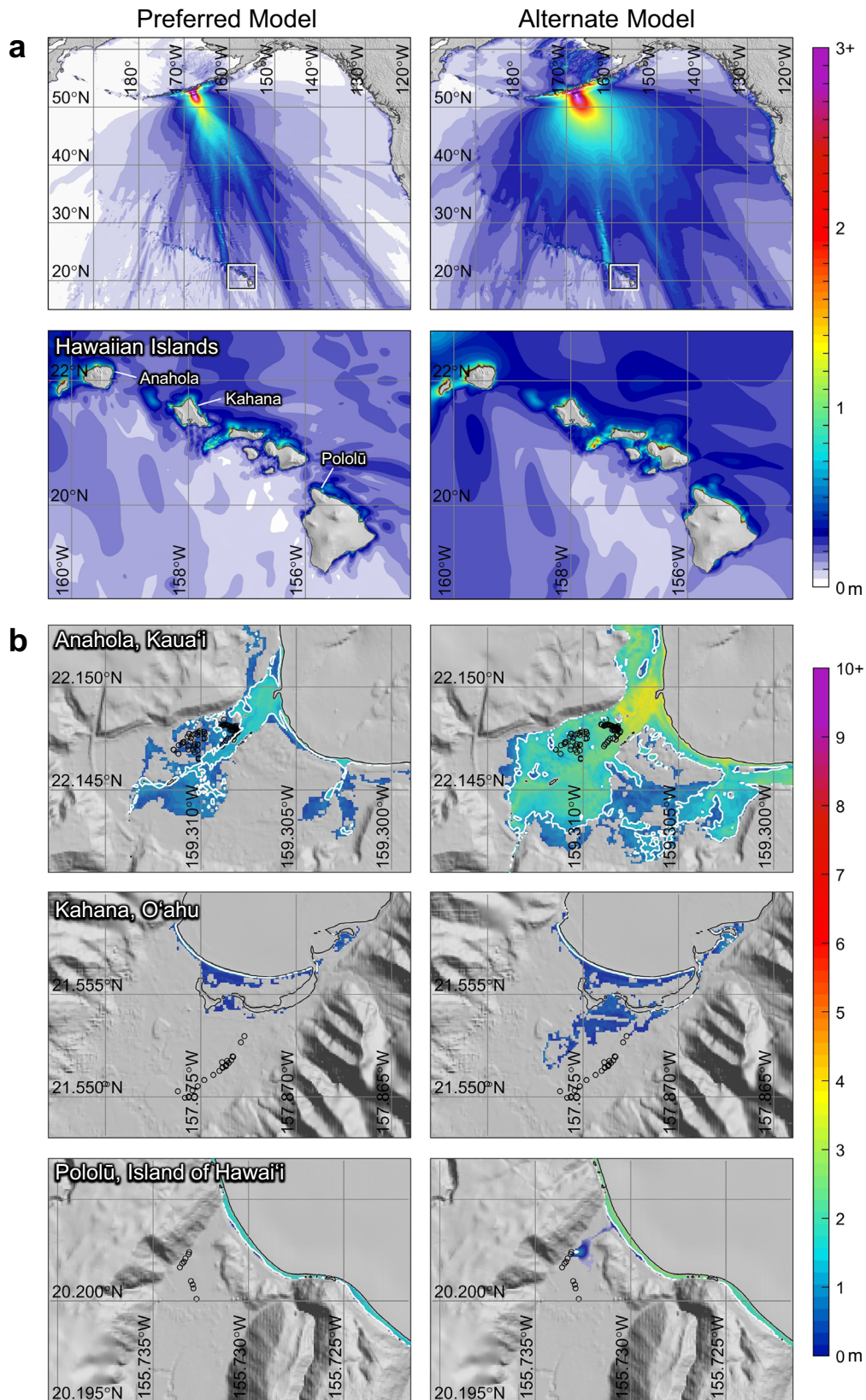


**Fig. 6 | Models for the 15<sup>th</sup> century far-field tsunami. a** Tsunami wave amplitude. White rectangles in upper panels delineate the Hawai'i region with higher resolution results shown in lower panels. **b** Computed flow depth and stratigraphic records at Hawai'i sites. Base maps generated from [https://www.gebco.net/data\\_and\\_products/gridded\\_bathymetry\\_data/](https://www.gebco.net/data_and_products/gridded_bathymetry_data/) and <https://www.ncei.noaa.gov/maps/bathymetry/>. Black lines denote waterlines at adjusted local mean sea level according to Table 1 and white lines denote 1-m flow depth. Solid white and open circles mark the location of cores with and without coeval tsunami deposits (Source data available from <https://doi.org/10.5066/P9X4STJM>).

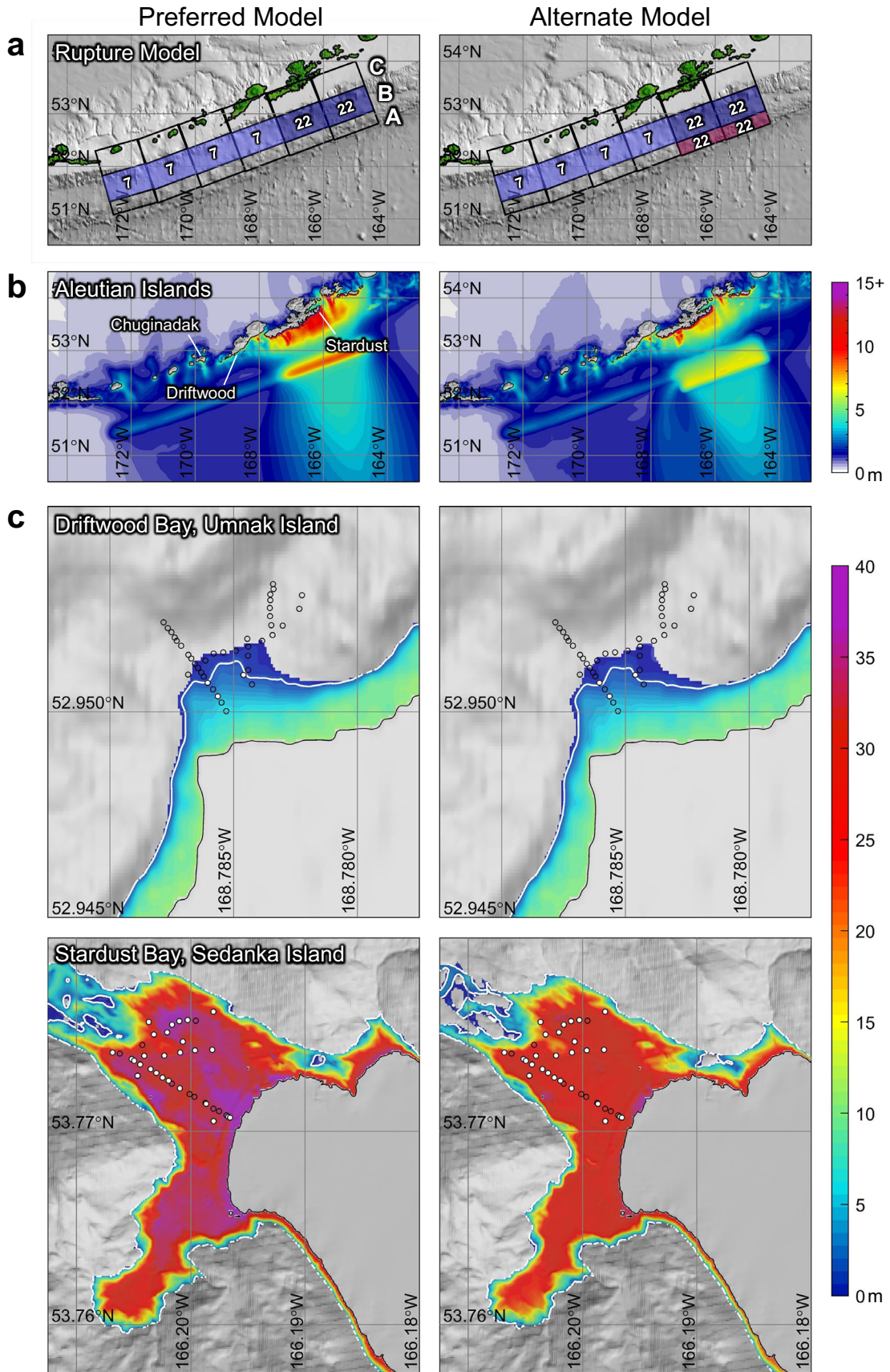


**Fig. 7 | Models for the 14<sup>th</sup> century rupture and near-field tsunami. a** Rupture model. Red and blue tones denote shallow and deeper megathrust slip in meters. **b** Near-field tsunami amplitude. **c** Computed flow depth and stratigraphic records at Aleutian sites. Base maps generated from <https://www.ncei.noaa.gov/maps/>

[bathymetry](https://www.ncei.noaa.gov/maps/). Black lines denote waterlines at present local mean sea level and white lines denote 1-m flow depth. Solid white and open circles mark the location of cores with and without coeval tsunami deposits (Source data available from <https://doi.org/10.5066/P9D7KLVJ>).

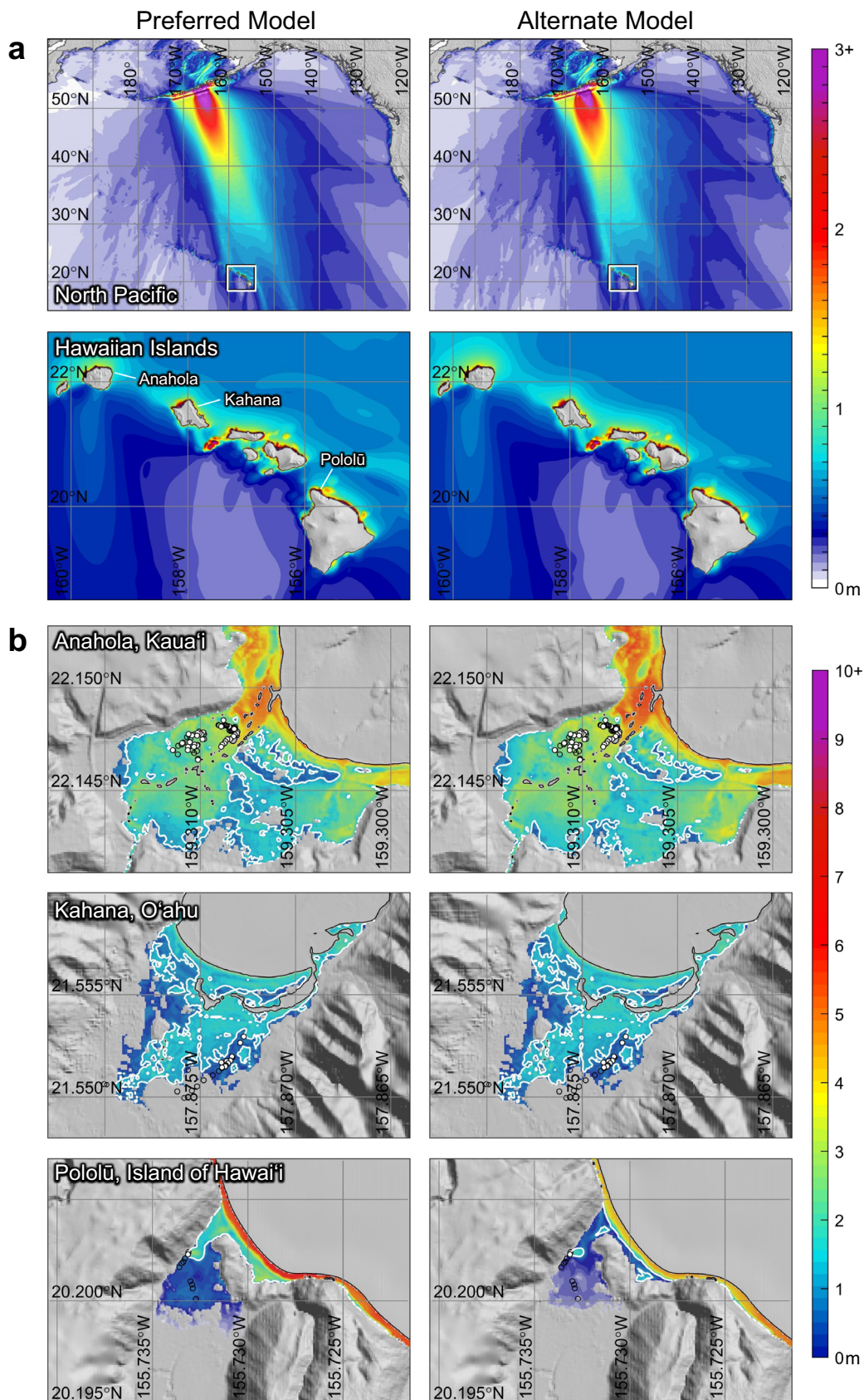


**Fig. 8 | Models for the 14<sup>th</sup> century far-field tsunami. a** Tsunami wave amplitude. White rectangles in upper panels delineate the Hawai'i region with higher resolution results shown in lower panels. **b** Computed flow depth and stratigraphic records at Hawai'i sites. Base maps generated from [https://www.gebco.net/data\\_and\\_products/gridded\\_bathymetry\\_data/](https://www.gebco.net/data_and_products/gridded_bathymetry_data/) and <https://www.nci.noaa.gov/maps/>

[bathymetry/](https://www.gebco.net/data_and_products/gridded_bathymetry_data/). Black lines denote waterlines at adjusted local mean sea level according to Table 1 and white lines denote 1-m flow depth. Solid white and open circles mark the location of cores with and without coeval tsunami deposits (Source data available from <https://doi.org/10.5066/P9X4STJM>).

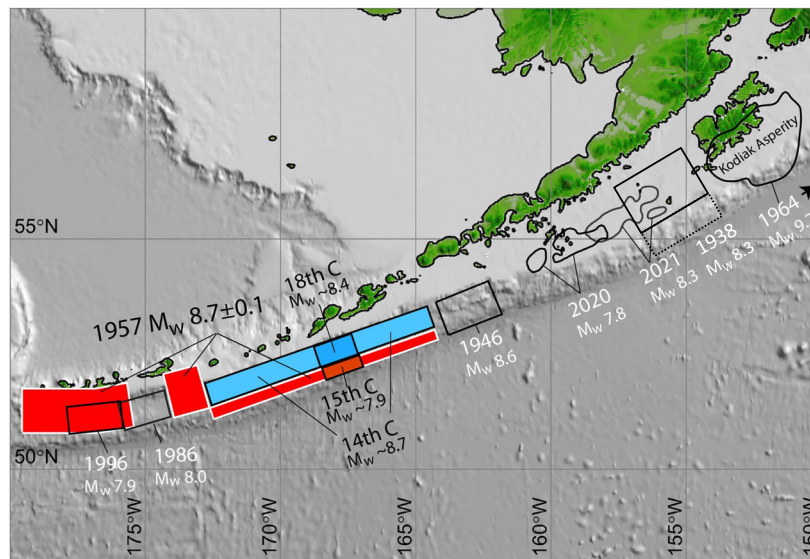


**Fig. 9 | Large coseismic-slip regions along the Aleutian Islands and Alaska Peninsula.** The Kodiak Asperity has greater than 4 m slip in the western portion of the 1964 Alaska earthquake rupture<sup>56</sup>; the 1938 rupture<sup>23</sup> has 2 m slip and limited shallow slip of 1 m delineated by dotted lines; and the 2020 Simeonof and 2021 Chignik source regions have greater than 0.5 and 2 m slip<sup>21,57</sup>. The 1946 and 1986 rupture zones have greater than 8 and 2 m slip<sup>17,58</sup>, while the 1996 rupture has 2 m

slip<sup>59</sup>. The 1957 rupture has 1.5–4.3 m slip in the western region and 12–26 m in the east<sup>3</sup>. Base map generated from [https://www.gebco.net/data\\_and\\_products/gridded\\_bathymetry\\_data/](https://www.gebco.net/data_and_products/gridded_bathymetry_data/). The 15<sup>th</sup> century event with 32 m slip overlaps the 1957 shallow slip zone demonstrating re-rupture of a tsunami earthquake, while the 14<sup>th</sup> and overlapping 18<sup>th</sup> century events have up to 26 and 22 m slip down-dip from the shallow rupture in 1957.

because sediment deposit is only present in one of a row of closely spaced cores. The modeled inundation extends farther inland than the deposits in Kahana Valley, but has less than 1 m flow depth at those cores. As the upper-bound inundation is not well constrained by the Stardust and Anahola sites, a dramatic increase of the eastern slip can generate the required flow depth at the Kahana deposit locations. In comparison, the updated 1957 rupture model<sup>3</sup> does not produce inundation at the cores in Kahana Valley consistent with the lack of corresponding deposits. The most severe 1946 tsunami in Hawaii's recorded history also did not have deposits at the Kahana cores (Fig. 2). These factors along with the timing uncertainty negate the use of the Kahana record as the primary constraint for slip along the eastern 200 km segment of the 14<sup>th</sup> century rupture model.

Placing the 14<sup>th</sup> century slip in the domain B region of the rupture grid produces subsidence along the shelf edge and uplift on the upper continental slope. The free surface upswing following the initial draw-down at the shelf edge coincides with arrival of the initial pulse generated by the continental slope uplift. The constructive interference increases the wave amplitude over the shelf and runup at the Aleutian shore. This local resonance ceases to occur for a wider rupture zone and provides an indirect constraint on the along-dip slip extent when one of the criteria is to match the inferred runup with the least subfaults. As a demonstration, we provide an alternate model with the eastern rupture off Stardust Bay extended to the trench (Fig. 7a). This model produces subsidence along the upper continental slope and extends the uplift to the trench, but has less inundation at Stardust Bay despite having a larger seismic moment (Fig. 7c), partly because the upswing from the initial drawdown is no longer aligned with the initial arrival from the lower continental slope. The slip extension to the trench also results in a smaller-amplitude, wider initial pulse over deeper water<sup>32</sup> on the east side (Fig. 7b) that reduces the impact in the near field and steers the offshore tsunami westward (Fig. 8a). The computed inundation is slightly more severe at the Anahola site, but notably less at Pololū compared to the preferred model (Fig. 8b). Placing large shallow slip off Stardust Bay is viable as the region is outside of the inferred 15<sup>th</sup> century rupture, but the higher seismic moment involving additional subfaults makes this model less favorable based on the selection criterion of providing a lower-bound estimate.

## Discussion

Inundation modeling constrained by stratigraphic records can provide additional details for understanding of subduction zone processes and assessment of tsunami hazards. The inferred great ruptures in the 14<sup>th</sup>, 15<sup>th</sup>, and 18<sup>th</sup> centuries are summarized in Fig. 9 along with the updated 1957 rupture model<sup>3</sup> and instrumentally recorded major events in adjacent segments. The models suggest that peak slip of 22–32 m has occurred in multiple events in the eastern Aleutian subduction zone, alternating between Domains A and B in the central and near-trench regions. The overall earthquake recurrence interval is 100–300 years, but segments of the central and near-trench faults appear to re-rupture with intervals of 400–500 years, essentially balancing the interplate strain accumulation estimated from the current convergent rate<sup>1</sup>. The inferred sequence of alternating ruptures across the megathrust adds to the evidence of recurring tsunami earthquakes along a shallow plate boundary<sup>40</sup> that can produce large tsunamis despite the relatively weak ground shaking felt near the source<sup>41</sup>.

The plate boundary along Umnak Island with inferred large slip appears to have strong coupling in the central and shallow domains, but recent geodetic inferences only resolve moderate strain accumulation in the former<sup>7–9</sup>. Lower coupling of the central domain appears likely along other portions of the eastern Aleutian Islands, but there is uncertainty because occurrence of re-rupture remains an unknown, especially toward the west due to lack of local stratigraphic records. Even with a 700-year sequence of great earthquakes, there is still insufficient information to infer the coupling strength over the entire region. The Domain B rupture in the western portion of the 1957 event was overlapped by large ruptures in 1986 and 1996, but prior rupture of the 1946 zone to the east has not been documented (Fig. 9). The well-resolved slip distributions for 2020 and 2021 ruptures along the Alaska Peninsula have some overlap with prior events in 1917 and 1938, respectively, but the coupling of the shallow megathrust in both regions remains unresolved. In general, inferring megathrust seismic potential based on the short seismological histories available in many subduction zones is intrinsically uncertain, especially regarding potential for near-trench failures up-dip of deeper ruptures. More land-based and seafloor geodetic observations and additional

stratigraphic records are needed to better resolve plate boundary coupling and assess long-term tsunami hazards.

The tropical wetland environments of Hawai'i may have a higher flow depth threshold for tsunami deposit preservation compared to the Aleutian sites. The modeled tsunamis from the 14<sup>th</sup>, 15<sup>th</sup>, and 18<sup>th</sup> century sources show considerable inundation in Hawai'i despite absence of coeval deposits from the 15<sup>th</sup> and 18<sup>th</sup> century events. If the Hawai'i sites are only recording geologic evidence of the largest tsunamis, but still experience significant inundation from other Aleutian sources, the stratigraphic records alone underestimate the tsunami hazards. The correlation of paleotsunami deposits between the Aleutian and Hawai'i sites is also limited by the uncertainties in radiocarbon dating (Fig. 2). Testing earthquake sources and modeling tsunami inundation in both the near and far fields are complementary in differentiating plausible events. For example, the single paleotsunami deposit observed in Kahana Valley overlaps in age with both the 14<sup>th</sup> and 15<sup>th</sup> century deposits in Driftwood Bay. The preferred 15<sup>th</sup> century source model matches the stratigraphic records at the two Aleutian sites without inundation beyond the Kahana shore, while the preferred 14<sup>th</sup> century event produces severe inundation in the valley with minor flooding at the deposit locations. Although we still cannot definitively rule out a 15<sup>th</sup> century age for the Kahana Valley paleotsunami deposits, the modeling suggests the deposit was more likely from the 14<sup>th</sup> century tsunami.

Despite the relatively recent 1946 and 1957 events, tsunamis from the eastern Aleutian subduction zone remain a continuing threat to coastal communities in Hawai'i and Alaska. The preferred rupture models for the three prehistoric great earthquakes with strong stratigraphic signatures in the near field complemented by records in Hawai'i provide lower-bound estimates of megathrust slip and rupture extent. The computed inundation for the most severe 14<sup>th</sup> century Domain-B rupture exceeds the level of the 1957 Aleutian tsunami generated by near-trench Domain-A slip<sup>3</sup>. Portions of Domain B might have acquired sufficient strain in the last few centuries to rupture again. Together with the updated 1957 model<sup>3</sup>, the inferred 700-year rupture sequence provides useful information to develop logic trees of recurring great earthquakes in the eastern Aleutian subduction zone for probabilistic assessment of tsunami hazards in Hawai'i and critical facilities in the Aleutian Islands. Despite the low population density, Dutch Harbor on Unalaska Island is one of the largest fishing ports in the US. Such information is particularly important for defining low-probability earthquake and tsunami scenarios, which are used in engineering design, critical infrastructure siting, and evacuation planning.

Recent geodetic measurements<sup>7–9,20</sup> along the eastern Aleutian Islands do not appear to detect very shallow strain accumulation that leads to tsunami earthquakes like the 15<sup>th</sup> century, 1946, and 1957 events (Fig. 9). Apart from the complex upper-plate processes and their large distance from the trench, this might result from the Domain A region being relatively early into a 400–500 year cycle since the recent ruptures<sup>42</sup>. The updated 1957 model<sup>3</sup> indicates rupture of the near-trench, Domain A region with considerable slip, but shows no clear resolution of slip in the deeper Domain B. Consistent with geodetic measurements, contemporary strain accumulation at the central depth range of the megathrust is likely ongoing since the 18<sup>th</sup> century rupture over at least a relatively short segment of the Domain B region along Umnak Island. The inferred alternating rupture chronology suggests the eastern Aleutian subduction zone may produce a major Domain B earthquake and tsunami similar to the 14<sup>th</sup> century event in the future, especially with the stress increase likely to have been imparted on the central megathrust by the large shallow 1957 slip<sup>43</sup>.

## Methods

The inference of prehistoric earthquake ruptures from tsunami deposits involves a multidisciplinary approach with methods from coastal sedimentary geology, solid-earth geophysics, and ocean wave dynamics. These include interpretation of stratigraphic records as

constraints for tsunami modeling, development of rupture models representative of the eastern Aleutian subduction zone, accurate modeling of far- and near-field tsunami processes, and assessment of morphological and sea-level changes since the prehistoric events.

## Stratigraphic records

We compiled coastal geological evidence for paleotsunami inundation in the Aleutian and Hawaiian Islands<sup>23–25,29</sup> to assess a variety of rupture scenarios for the eastern Aleutian subduction zone. Sandy deposits, recording tsunami inundation, were examined in trenches and sediment cores, and described in the field. The ages of stratigraphic contacts were evaluated using C-14 and Cesium-137 analyses. The positions of trenches, cores, and drift logs in the Aleutian Islands were measured using real-time kinematic Global Navigation Satellite System (RTK GNSS) survey instruments with  $\pm 1.5$  cm horizontal and  $\pm 3$  cm vertical accuracy. Elevations are referenced to present mean sea level, which is determined at each site from water level measurements using pressure transducers and the National Tidal Datum Epoch. In the Hawaiian Islands, handheld GPS units provided all core locations within a horizontal error of  $\pm 4$  m. An RTK GNSS survey instrument was used to measure core elevations in Anahola Valley. Core elevations in Kahana and Pololū Valleys were estimated from LiDAR data with a vertical error of  $\pm 15$  cm.

Two sites in the eastern Aleutian Islands provide important constraints on near-field tsunami inundation from prehistoric Aleutian earthquakes (Fig. 2). The sites are on separate islands in open embayments that face the Pacific Ocean. Stardust Bay on Sedanka Island, located 25 km southeast of Dutch Harbor, contains evidence for 6 tsunamis in the past 1700 years, including geologic evidence from the 1957 earthquake and tsunami<sup>23</sup>. On Umnak Island, located 180 km southwest of Dutch Harbor, evidence for 8 tsunamis in the past 2000 years comes from Driftwood Bay<sup>24</sup>. Both locations have abundant sediment supply and well-preserved deposits across the valley for comparison with the computed inundation pattern. Additional undated tsunami deposit observations are available on Chuginadak Island 70 km west of Driftwood Bay<sup>25</sup>. Multiple cores show at least three tsunami deposits beneath the 1957 layer that can provide a reference for slip placement and model selection.

Up to 4000 kilometers south of the eastern Aleutian Islands, sites on three Hawaiian Islands record marine sand beds that are interpreted to have been deposited during inundation by far-field tsunamis generated in the Aleutian Islands in the 14<sup>th</sup> or 15<sup>th</sup> century, 1946 CE, and 1957 CE<sup>29</sup>. These sites are located in northeast-facing valleys containing coastal marsh records at least 1000-year old. Anahola Valley, Kaua'i, and Pololū Valley, Island of Hawai'i, both contain tsunami deposits from a 14<sup>th</sup> century event in addition to deposits from the 1946 and 1957 tsunamis, while Kahana Valley, O'ahu only contains geologic evidence from one prehistoric event in either the 14<sup>th</sup> or 15<sup>th</sup> century (Fig. 2). Because the sedimentary evidence from far-field tsunamis in Hawai'i is only preserved in low-lying and relatively flat depositional environments, runup heights and inundation limits inferred from tsunami deposits represent a lower-bound estimate of the impact. Runup heights derived from the preserved sandy deposits for all three tsunamis are less than 2.5 m above present mean sea level. The inland extent of the tsunami deposits is perhaps a better indicator of the minimum inundation. The paleotsunami deposits in Anahola, Kahana, and Pololū Valleys were observed, respectively, at up to 650, 480, and 260 m inland from modern shorelines.

One, or possibly two, paleotsunami deposits observed at the two Aleutian sites correlate in age with the paleotsunami deposit observed at each of the three Hawai'i sites (Fig. 2). At Anahola and Pololū Valleys, the 14<sup>th</sup> century deposits overlap in age with the 14<sup>th</sup> century deposits at the two Aleutian sites. At Kahana Valley, the two-sigma age uncertainty spans a century and overlaps in age with the 14<sup>th</sup> century event in the Aleutian Islands in addition to the 15<sup>th</sup> century event, which was only observed at Driftwood Bay. Although we cannot definitively rule out the 15<sup>th</sup> century

timing of the Kahana Valley paleotsunami deposit, the tsunami modeling links the near and far-field geologic records for inference of rupture models as well as query of data uncertainty and interpretation.

### Rupture and Tsunami models

The rupture and tsunami models work as an integrated system to transfer a fault-slip distribution to coastal inundation for use in matching the stratigraphic records. Space-time evolution of slip during earthquake rupture can be resolved with a finite-fault model using seismic, geodetic, and tsunami measurements. This usually requires time series signals to resolve detailed rupture kinematics over a fine grid of subfaults<sup>21,41,44</sup>. Given the lack of instrumental waveform information in this study, we take a first-order approach with larger subfaults by adopting the eastern half of the rupture grid used in the updated 1957 model<sup>3</sup> (Fig. 1). The 3 by 6 grid of subfaults follows the Slab2 plate interface model<sup>45</sup> along and across the eastern Aleutian subduction zone. The three rows of 100-km long subfaults with 30, 60, and 60 km width and 15°, 20°, and 25° dip correspond to the near-trench, central, and down-dip regions, which reflect the depth-dependent rupture and tsunamigenic properties across the megathrust<sup>10</sup>. For modeling of tsunami excitation, the rupture is assumed to start simultaneously across the entire fault and the dislocation follows a linear function over a 40 sec rise time to reach the specified slip.

The tsunami code NEOWAVE augments the commonly used non-linear shallow-water equations with depth-averaged vertical velocity and nonhydrostatic pressure<sup>31,32</sup>. The resulting quasi three-dimensional flow enables description of tsunami generation from time-dependent seafloor deformation, frequency dispersion during trans-oceanic propagation, and wavenumber-dependent shoaling on seafloor slopes. The vertical inertia facilitates accurate description of sea-surface oscillation as well as runup and drawdown on steep topography<sup>46</sup>. A shock-capturing scheme approximates breaking waves as bores or hydraulic jumps to ensure conservation of mass and momentum while enabling energy dissipation without predefined mechanisms. These model capabilities have been benchmarked against mathematical and numerical models as well as laboratory and field measurements<sup>47</sup>. The vertical velocity term also provides a direct interface with fault-slip models of prescribed subfault dislocation and rise time, which in turn provide the time history of earth surface deformation through an elastic half-space solution<sup>48</sup>. The seafloor vertical displacement is adjusted for horizontal translation of the local slope<sup>36</sup> to define the tsunami excitation and update the digital elevation model (DEM).

The modeling involves five levels of two-way nested computational grids with increasing resolution from the open ocean to the sites with stratigraphic records (Supplementary Fig. 1). The level-1 grid covers the north Pacific and the 2-arcmin resolution leads to optimal model dispersion for transoceanic tsunami propagation<sup>49</sup>. Two level-2 grids resolve shelf and slope complexes along the Aleutian and Hawaiian Islands at 30 arcsec. The level-3 to 5 grids telescope from 6 to 0.3 arcsec resolution for inundation modeling at each stratigraphic record site. Manning's numbers of 0.025 and 0.035 describe subgrid roughness of the seafloor and terrain<sup>50</sup>. The DEM includes GEBCO for the North Pacific Ocean and high-resolution bathymetry and topography from NOAA NCEI for the Aleutian and Hawaiian Islands. A highway embankment along the Kahana shore is manually removed and the topography is interpolated from adjacent cells. The present, local mean sea level is the DEM datum, and along with applicable adjustments for long-term sea-level changes, provides the initial sea-surface elevation for inundation modeling of each prehistoric tsunami event.

### Morphological and sea-level changes

The computational grids incorporate the present-day bare-earth topography referenced to mean-sea level. A major source of uncertainty is the degree of shoreline and sea level changes that has occurred at specific paleotsunami sites. At Driftwood Bay in the Aleutian Islands, coastal

geomorphology and stratigraphy indicate that relative sea level and the position of past shorelines varied little in the past 2000 years. Terrestrial sediment buries ancient beach deposits and implies a <40 m seaward shift of the shoreline under conditions of stable or slowly falling (0.5 mm/yr) sea level<sup>24</sup>. At Stardust Bay, the shoreline has been within 200–300 m of the present position in the past 1600 years under similar conditions of stable or slowly rising sea level<sup>23</sup>. Since the 14<sup>th</sup> century, the time period of interest for the paleotsunamis study, sea level at the eastern Aleutian sites has remained stable or varied by  $\pm 0.35$  m. Over the same time period shoreline change has varied from a seaward shift of -14 m at Driftwood Bay to less than 200 m at Stardust Bay, likely a function of differences in sediment supply at the two sites. These uncertainties are small compared to the runup and inundation inferred from the stratigraphic records. The present-day topography and mean-sea level are used in modeling of prehistoric tsunamis at the Driftwood and Stardust sites.

At Pololū, Kahana, and Anahola Valleys in Hawai'i, the precise positions of shorelines and stream channels are not known at the time of tsunami inundation. However, the stratigraphy at these sites indicates that low-lying, coastal wetland environments were prevalent throughout the valleys over at least the last couple millennia. Subsidence of the Island of Hawai'i due to loading by active volcanoes, in addition to eustatic sea-level rise, has led to the infilling of Pololū Valley since the last glacial maximum<sup>51</sup>. Marsh peats have been accreting in Pololū Valley for at least the past 1700 years at an average rate of roughly 2 mm/yr<sup>29</sup>. In Kahana and Anahola Valleys, the window of time where sedimentary evidence of large paleotsunamis could have been preserved in wetland environments is shorter. Relatively young wetland sediments mantle prograding coastal plain sediments that formed as sea level dropped -2 m following the mid-Holocene Kapapa highstand<sup>52,53</sup>. While all three valleys have human settlement and cultivation activity, Pololū has experienced less anthropogenic modifications in the past half century relative to Anahola and Kahana. Presence of private properties and thick vegetation also limits the available locations for coring at the Hawai'i sites.

We correct modern DEMs used in tsunami inundation modeling at the Hawai'i sites by accounting for the difference in observed sediment accumulation and estimates of relative sea level in the 14<sup>th</sup> century<sup>54,55</sup>. The thickness of sediments above the 14<sup>th</sup> century tsunami deposits, which is 1.24 m in Pololū, 1.27 m in Kahana, and 1.31 m in Anahola Valleys, indicates accumulation of wetland sediments over the last ~700 years. Tide gauge data in Hawai'i demonstrate relative sea level rise over the last half-century to century at a rate of 3.5, 1.8, and 1.4 mm/year in Hilo Harbor, Island of Hawai'i; Honolulu Harbor, O'ahu; and Nāwiliwili Harbor, Kaua'i. These rates include flexural subsidence or uplift and eustatic sea level rise. We extrapolate these rates to the 14<sup>th</sup> century to determine the sea level at the time of paleotsunami inundation, which predicts relative sea levels at 2.35, 1.21, and 0.95 m lower than the present. We assume a constant deposition rate since the 14<sup>th</sup> century and similarly extrapolate modern sea level rise to roughly estimate relative sea levels in the 15<sup>th</sup> and 18<sup>th</sup> centuries. The difference between these predicted sea levels and the observed sediment accumulation is used to vertically shift modern DEMs (Table 1), in a rough reconstruction of the marsh surface elevations relative to sea level since the 14<sup>th</sup> century. This assumes that the shoreline position and beach or dune morphology were similar to today.

**Table 1 | Mean sea level adjustments for inundation modeling at Hawai'i sites**

	Mean sea level adjustment (m)		
	14 <sup>th</sup> Century	15 <sup>th</sup> Century	18 <sup>th</sup> Century
Anahola, Kaua'i	+0.35	+0.25	+0.10
Kahana, O'ahu	+0.05	–	–
Pololū, Island of Hawai'i	-1.10	-0.90	-0.55

Another source of uncertainty is the elevation of the paleotsunami deposits relative to tide level during past events. At the Unalaska and Nikolski stations nearest to Stardust and Driftwood Bays, the tidal range varies from 1.098 to 1.219 m, respectively. The highest deposit elevations are 13.3, 23.0, and 23.0 m above present mean sea level for the 14<sup>th</sup>, 15<sup>th</sup>, and 18<sup>th</sup> century events in Driftwood Bay and 14.3 and 14.4 m for the 14<sup>th</sup> and 18<sup>th</sup> century events in Stardust Bay. There is no sedimentary evidence for the 15<sup>th</sup> century event at Stardust Bay, where cores were collected from a beach-ridge strand plain fronted by a -7-m high beach berm. If the 15<sup>th</sup> century tsunami struck Stardust Bay, it did not overtop the barrier beach berm. The tidal amplitudes given by half of the tide ranges are an order magnitude smaller compared to the inferred runup and are well within the error bound of the analysis. The tide ranges of 0.558, 0.646, and 0.642 m at the Nāwiliwili, Moku O lo'e, and Kawaihae stations nearest to Anahola, Kahana, and Polulū are smaller compared to their Aleutian counterparts. The deposit elevations for the 14<sup>th</sup> century event in Hawai'i are up to 2.5 m above present mean sea level. Overall, the tidal amplitudes are small compared to the inferred runup and are within the uncertainty of model parameters.

### Reporting summary

Further information on research design is available in the Nature Portfolio Reporting Summary linked to this article.

### Data availability

Digital elevation models are available from [https://www.gebco.net/data\\_and\\_products/gridded\\_bathymetry\\_data/](https://www.gebco.net/data_and_products/gridded_bathymetry_data/) and <https://www.ncei.noaa.gov/maps/bathymetry/>, and the subduction zone geometry model<sup>45</sup> from <https://www.sciencebase.gov/catalog/item/5aa1b00ee4b0b1c392e86467>. Tsunami geology datasets<sup>23,24,29</sup> are available from U.S. Geological Survey data release: <https://doi.org/10.5066/P9D7KLJV> and <https://doi.org/10.5066/P9X4STJM>.

### Code availability

The code for tsunami modeling may be requested from the corresponding author for academic research.

### References

- DeMets, C., Gordon, R. G. & Argus, D. F. Geologically current plate motions. *Geophys. J. Int.* **181**, 1–80 (2010).
- Sykes, L. R., Kisslinger, J. B., House, L. S., Davies, J. N. & Jacob, K. H. Rupture zones of great earthquakes in the Alaska-Aleutian arc, 1784 to 1980. *Science* **210**, 1343–1345 (1980).
- Yamazaki, Y. et al. A great tsunami earthquake component of the 1957 Aleutian Islands earthquake. *Earth Planet. Sci. Lett.* **637**, 118692 (2024).
- Tape, C. & Lomax, A. Aftershock regions of Aleutian-Alaska megathrust earthquakes, 1938–2021. *J. Geophys. Res. Solid Earth* **127**, e2022JB024336 (2022).
- Lander, J. F. Tsunamis Affecting Alaska, 1737–1996. US Department of Commerce, National Oceanic and Atmospheric Administration, National Geophysical Data Center, Geophysical Research Documentation No. 31, Boulder, Colorado (1996).
- Butler, R., Burney, D. A. & Walsh, D. Paleotsunami evidence on Kaua'i and numerical modeling of a great Aleutian tsunami. *Geophys. Res. Lett.* **41**, 6795–6802 (2014).
- Cross, R. S. & Freymueller, J. T. Evidence for and implications of a Bering plate based on geodetic measurements from the Aleutians and western Alaska. *J. Geophys. Res.* **113**, B07405 (2008).
- Freymueller, J. T. et al. Active deformation processes in Alaska, based on 15 years of GPS measurements. In: *Active Tectonics and Seismic Potential of Alaska*, Geophysical Monograph Series, vol. 179, (eds Freymueller, J. T., Haeussler, P. J., Wesson, R. & Ekström, G.) 1–42 (American Geophysical Union, 2008).
- Elliott, J. & Freymueller, J. A block model of present-day kinematics of Alaska and western Canada. *J. Geophys. Res. Solid Earth* **125**, e2019JB018378 (2020).
- Lay, T. et al. Depth-varying rupture properties of subduction zone megathrust faults. *J. Geophys. Res. Solid Earth* **117**, B04311 (2012).
- Holbrook, W. S. H., Lizarralde, D., McGeary, S. & Bangs, N. J. Deibold, Structure and composition of the Aleutian island arc and implications for continental crustal growth. *Geology* **27**, 31–34 (1999).
- Lizarralde, D., Holbrook, W. S., McGeary, S., Bangs, N. & Diebold, J. Crustal construction of a volcanic arc, wide-angle seismic results from the western Alaska Peninsula. *J. Geophys. Res.* **107**, 2164 (2002).
- Kanamori, H. Mechanism of tsunami earthquakes. *Phys. Earth Planet. Int.* **6**, 346–359 (1972).
- Polet, J. & Kanamori, H. Shallow subduction zone earthquakes and their tsunamigenic potential. *Geophys. J. Int.* **142**, 684–702 (2000).
- Lay, T. & Bilek, S. L. Anomalous earthquake ruptures at shallow depths on subduction zone megathrusts. In: *The Seismogenic Zone of Subduction Zone Thrust Faults* (eds Dixon, T. H. & Moore, J. C.) 476–511 (Columbia University Press, 2007).
- Pelayo, A. M. *Earthquake source parameter inversion using body and surface waves: applications to tsunami earthquakes and to Scotia Sea seismotectonics*. PhD Thesis, (Washington University, St. Louis, 1990).
- López, A. M. & Okal, E. A. A seismological reassessment of the source of the 1946 Aleutian 'tsunami' earthquake. *Geophys. J. Int.* **165**, 835–849 (2006).
- Okal, E. A., Plafker, G., Synolakis, C. E. & Borrero, J. C. Near-field survey of the 1946 Aleutian tsunami on Unmak and Sunak Islands. *Bull. Seism. Soc. Am.* **93**, 1226–1234 (2003).
- Walker, D. Regional Tsunami evacuations for the state of Hawaii: A feasibility study on historical runup data. *Sci. Tsunami Hazards* **22**, 3–22 (2004).
- Li, S. & Freymueller, J. T. Spatial variation of slip behavior beneath the Alaska Peninsula along Alaska-Aleutian subduction zone. *Geophys. Res. Lett.* **45**, 3453–3460 (2018).
- Bai, Y., Liu, C., Lay, T., Cheung, K. F. & Ye, L. Optimizing a model of coseismic rupture for the 22 July 2020  $M_w$  7.8 Simeonof earthquake by exploiting acute sensitivity of tsunami excitation across the shelf break. *J. Geophys. Res. Solid Earth* **129**, e2002JB024484 (2022).
- Bai, Y. et al. Limited shallow slip in the 1938  $M_S$  8.3 Alaska Peninsula earthquake rupture. *Geophys. Res. Lett.* **52**, e2024GL113880 (2025).
- Witter, R. C. et al. Unusually large tsunamis frequent a currently creeping part of the Aleutian megathrust. *Geophys. Res. Lett.* **43**, 76–84 (2016).
- Witter, R. C. et al. Evidence for frequent, large tsunamis spanning locked and creeping parts of the Aleutian megathrust. *Geol. Soc. Am. Bull.* **131**, 707–729 (2019).
- Griswold, F. R., MacInnes, B. T. & Higman, B. Tsunami-based evidence for large eastern Aleutian slip during the 1957 earthquake. *Quat. Res.* **91**, 1045–1058 (2019).
- Nicolsky, D. J., Freymueller, J. T., Witter, R. C., Suleimani, E. N. & Koehler, R. D. Evidence for shallow megathrust slip across the Unalaska seismic gap during the great 1957 Andreanof Islands earthquake, eastern Aleutian Islands, Alaska. *Geophys. Res. Lett.* **43**, 76–84 (2016).
- Johnson, J. M. & Satake, K. Source parameters of the 1957 Aleutian earthquake from tsunami waveforms. *Geophys. Res. Lett.* **20**, 1487–1490 (1993).
- Johnson, J. M. et al. The 1957 great Aleutian earthquake. *Pure Appl. Geophys.* **142**, 3–28 (1994).
- La Selle, S. et al. Sedimentary evidence of prehistoric distant-source tsunamis in the Hawaiian Islands. *Sedimentology* **67**, 1249–1273 (2020).
- House, L. S., Sykes, L. R., Davies, J. N. & Jacob, K. H. Identification of a possible seismic gap near Unalaska Island, eastern Aleutians,

- Alaska. In: *Earthquake Prediction - An International Review* (Simpson, D. W. & Richards, P. G.) 81–92 (AGU Maurice Ewing Series, 1981).
31. Yamazaki, Y., Kowalik, Z. & Cheung, K. F. Depth-integrated, non-hydrostatic model with grid nesting for tsunami generation, propagation, and run-up. *Int. J. Numer. Met. Fluids* **61**, 473–497 (2009).
  32. Yamazaki, Y., Cheung, K. F. & Kowalik, Z. Depth-integrated, non-hydrostatic model for wave breaking and run-up. *Int. J. Numer. Met. Fluids* **67**, 2081–2107 (2011).
  33. Namegaya, Y. & Satake, K. Reexamination of the A.D. 869 Jogan earthquake size from tsunami deposit distribution, simulated flow depth and velocity. *Geophys. Res. Lett.* **41**, 2297–2303 (2014).
  34. Apotsos, A. et al. Tsunami inundation and sediment transport in a sediment-limited embayment on American Samoa. *Earth Sci. Rev.* **107**, 1–11 (2011).
  35. Cheung, K. F., Bai, Y. & Yamazaki, Y. Surges around the Hawaiian Islands from the 2011 Tohoku tsunami. *J. Geophys. Res. Oceans* **118**, 5703–5719 (2013).
  36. Tanioka, Y. & Satake, K. Tsunami generation by horizontal displacement of ocean bottom. *Geophys. Res. Lett.* **23**, 861–864 (1996).
  37. Tanioka, Y. & Seno, T. Sediment effect on tsunami generation of the 1896 Sanriku tsunami earthquake. *Geophys. Res. Lett.* **28**, 3389–3392 (2001).
  38. Kanamori, H. & Kikuchi, M. The 1992 Nicaragua earthquake: a slow tsunami earthquake associated with subducted sediments. *Nature* **361**, 714–716 (1993).
  39. Cheung, K. F., Lay, T., Sun, L. & Yamazaki, Y. Tsunami size variability with rupture depth. *Nat. Geosci.* **15**, 33–36 (2022).
  40. Philibosian, B. et al. An ancient shallow slip event on the Mentawai segment of the Sunda megathrust, Sumatra. *J. Geophys. Res.* **117**, B05401 (2012).
  41. Lay, T. et al. The 25 October 2010 Mentawai tsunami earthquake ( $M_W$  7.8) and the tsunami hazard presented by shallow megathrust ruptures. *Geophys. Res. Lett.* **38**, L06302 (2011).
  42. Govers, R., Furlong, K. P., van de Wiel, L., Herman, M. W. & Broerse, T. The geodetic signature of the earthquake cycle at subduction zones: Model constraints on the deep processes. *Rev. Geophys.* **56**, 6–49 (2017).
  43. Xia, T. et al. The 2022  $M_W$  7.3 Southern Sumatra tsunami earthquake: Rupture up-dip of the 2007  $M_W$  8.4 Bengkulu event. *J. Geophys. Res. Solid Earth* **129**, e2024JB030284 (2024).
  44. Bai, Y., Liu, C., Lay, T., Cheung, K. F. & Yamazaki, Y. Fast and slow intraplate ruptures during the 19 October 2020 magnitude 7.6 Shumagin earthquake. *Nat. Comm.* **14**, 2015 (2023).
  45. Hayes, G. P. Slab2, a comprehensive subduction zone geometry model. *Science* **362**, 58–61 (2018).
  46. Bai, Y., Yamazaki, Y. & Cheung, K. F. Intercomparison of hydrostatic and nonhydrostatic modeling for tsunami inundation mapping. *Phys. Fluids* **35**, 077111 (2023).
  47. Yamazaki, Y., Bai, Y., Goo, L. L., Cheung, K. F. & Lay, T. Nonhydrostatic modeling of tsunamis from earthquake rupture to coastal impacts. *J. Hydraul. Eng.* **149**, 04023033 (2023).
  48. Okada, Y. Surface deformation due to shear and tensile faults in a half-space. *Bull. Seismol. Soc. Am.* **75**, 1125–1154 (1985).
  49. Li, L. & Cheung, K. F. Numerical dispersion in non-hydrostatic modeling of long-wave propagation. *Ocean Model.* **138**, 68–87 (2019).
  50. Bricker, J. D., Gibson, S., Takagi, H. & Imamura, F. On the need for larger Manning's roughness coefficients in depth-integrated tsunami inundation models. *Coast. Eng. J.* **57**, 1550005-1 (2015).
  51. Vitousek, P. M., Chadwick, O. A., Hilley, G., Kirch, P. V. & Ladefoged, T. N. Erosion, geological history, and indigenous agriculture: A tale of two valleys. *Ecosystems* **13**, 782–793 (2010).
  52. Calhoun, R. S. & Fletcher, C. H. III Late Holocene coastal plain stratigraphy and sea-level history at Hanalei, Kauai, Hawaiian Islands. *Quat. Res.* **45**, 47–58 (1996).
  53. Grossman, E. E. & Fletcher, C. H. III Sea level higher than present 3500 years ago on the northern main Hawaiian Islands. *Geology* **26**, 363–366 (1998).
  54. Yang, L. & Francis, O. P. Sea-level rise and vertical land motion on the Islands of Oahu and Hawaii, Hawaii. *Adv. Space Res.* **11**, 2221–2232 (2019).
  55. Parker, A. Rates of subsidence and relative sea level rise in the Hawaii Islands. *Nonlinear Eng.* **5**, 255–268 (2016).
  56. Ichinose, G., Somerville, P., Thio, H.-K., Graves, R. & O'Connell, D. Rupture processes of the 1964 Prince William Sound, Alaska, earthquake from combined inversion of seismic, tsunami, and geodetic data. *J. Geophys. Res.* **112**, B07306 (2007).
  57. Liu, C., Bai, Y., Lay, T., Feng, Y. & Xiong, X. Megathrust complexity and the up-dip extent of slip during the 2021 Chignik, Alaska Peninsula earthquake. *Tectonophysics* **854**, 229808 (2023).
  58. Boyd, T. M. & Nabelek, J. L. Rupture process of the Andreanof Islands earthquake of May 7, 1986. *Bull. Seismol. Soc. Am.* **78**, 1653–1573 (1988).
  59. Tanioka, Y. & González, F. I. The Aleutian earthquake of June 10, 1996 ( $M_w$  7.9) ruptured parts of the Andreanof and Delarof segments. *Geophys. Res. Lett.* **25**, 2245–2248 (1998).

## Acknowledgements

This study was supported by the National Tsunami Hazard Mitigation Program under National Oceanic and Atmospheric Administration grant number NA20NWS467006 to the University of Hawai'i via Hawai'i Emergency Management Agency. T. Lay was supported by the National Science Foundation under grant number EAR-1802364. S. La Selle and B. Jaffe were supported by the U.S. Geological Survey Coastal and Marine Hazards and Resources Program. R. Witter was supported by the U.S. Geological Survey Earthquake Hazards Program. Any use of trade, firm, or product names is for descriptive purposes only and does not imply endorsement by the U.S. Government. We thank Adrian Bender for his comments and suggestions that improved this paper. SOEST Contribution No. 11917.

## Author contributions

K.F.C. and B.E.J. conceived the idea, which was elaborated with T.L. and Y.Y., who in turn developed the rupture and tsunami models. S.L.S. and R.C.W. compiled the geologic data and BEJ estimated prehistoric sea levels. Y.Y. led the investigation with input from K.F.C. and T.L. K.F.C. administered the project and coordinated the preparation and revision of the paper with all coauthors.

## Competing interests

The authors declare no competing interests.

## Additional information

**Supplementary information** The online version contains supplementary material available at <https://doi.org/10.1038/s41467-025-57802-w>.

**Correspondence** and requests for materials should be addressed to Kwok Fai Cheung.

**Peer review information** *Nature Communications* thanks Ignacio Sepulveda, Carl Tape and the other, anonymous, reviewer(s) for their contribution to the peer review of this work. A peer review file is available.

**Reprints and permissions information** is available at <http://www.nature.com/reprints>

**Publisher's note** Springer Nature remains neutral with regard to jurisdictional claims in published maps and institutional affiliations.

**Open Access** This article is licensed under a Creative Commons Attribution-NonCommercial-NoDerivatives 4.0 International License, which permits any non-commercial use, sharing, distribution and reproduction in any medium or format, as long as you give appropriate credit to the original author(s) and the source, provide a link to the Creative Commons licence, and indicate if you modified the licensed material. You do not have permission under this licence to share adapted material derived from this article or parts of it. The images or other third party material in this article are included in the article's Creative Commons licence, unless indicated otherwise in a credit line to the material. If material is not included in the article's Creative Commons licence and your intended use is not permitted by statutory regulation or exceeds the permitted use, you will need to obtain permission directly from the copyright holder. To view a copy of this licence, visit <http://creativecommons.org/licenses/by-nc-nd/4.0/>.

© The Author(s) 2025

## Supplementary Information for

### **A 700-year Rupture Sequence of Great Eastern Aleutian Earthquakes from Tsunami Modeling of Stratigraphic Records**

Yoshiki Yamazaki<sup>1</sup>, Kwok Fai Cheung<sup>1,✉</sup>, Thorne Lay<sup>2</sup>, SeanPaul M. La Selle<sup>3</sup>,  
Robert C. Witter<sup>4</sup>, and Bruce E. Jaffe<sup>3</sup>

<sup>1</sup>Department of Ocean and Resources Engineering, University of Hawai'i at Manoa, Honolulu, Hawai'i, 96822, USA. <sup>2</sup>Department of Earth and Planetary Sciences, University of California Santa Cruz, Santa Cruz, California, 95064, USA. <sup>3</sup>U.S. Geological Survey, Pacific Coastal and Marine Science Center, Santa Cruz, California, 95060, USA. <sup>4</sup>U.S. Geological Survey, Alaska Science Center, Anchorage, Alaska, 99508, USA.

#### **This PDF file includes:**

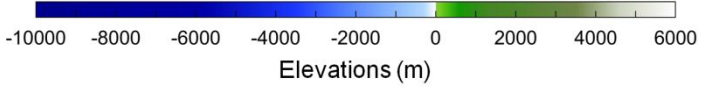
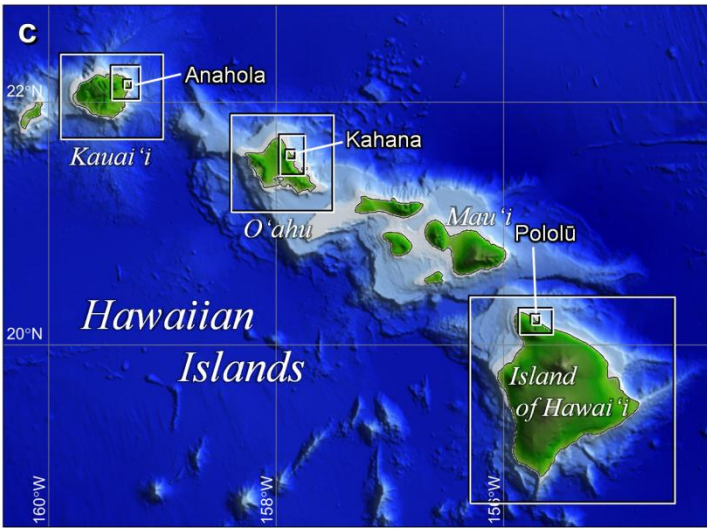
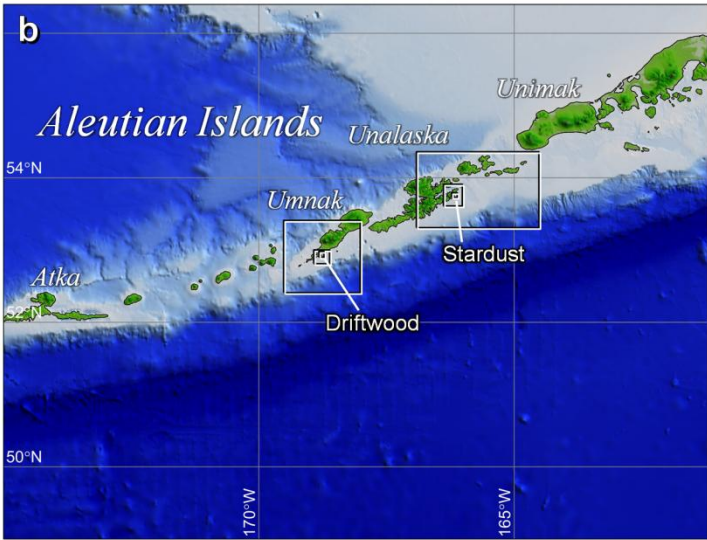
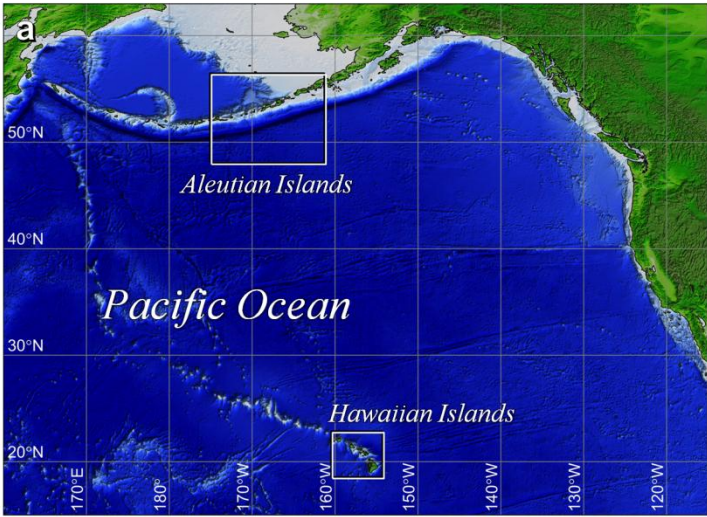
Supplementary Figure 1  
Supplementary Movies 1 to 3 (captions and snapshots)

#### **Other Supplementary Information for this manuscript includes the following:**

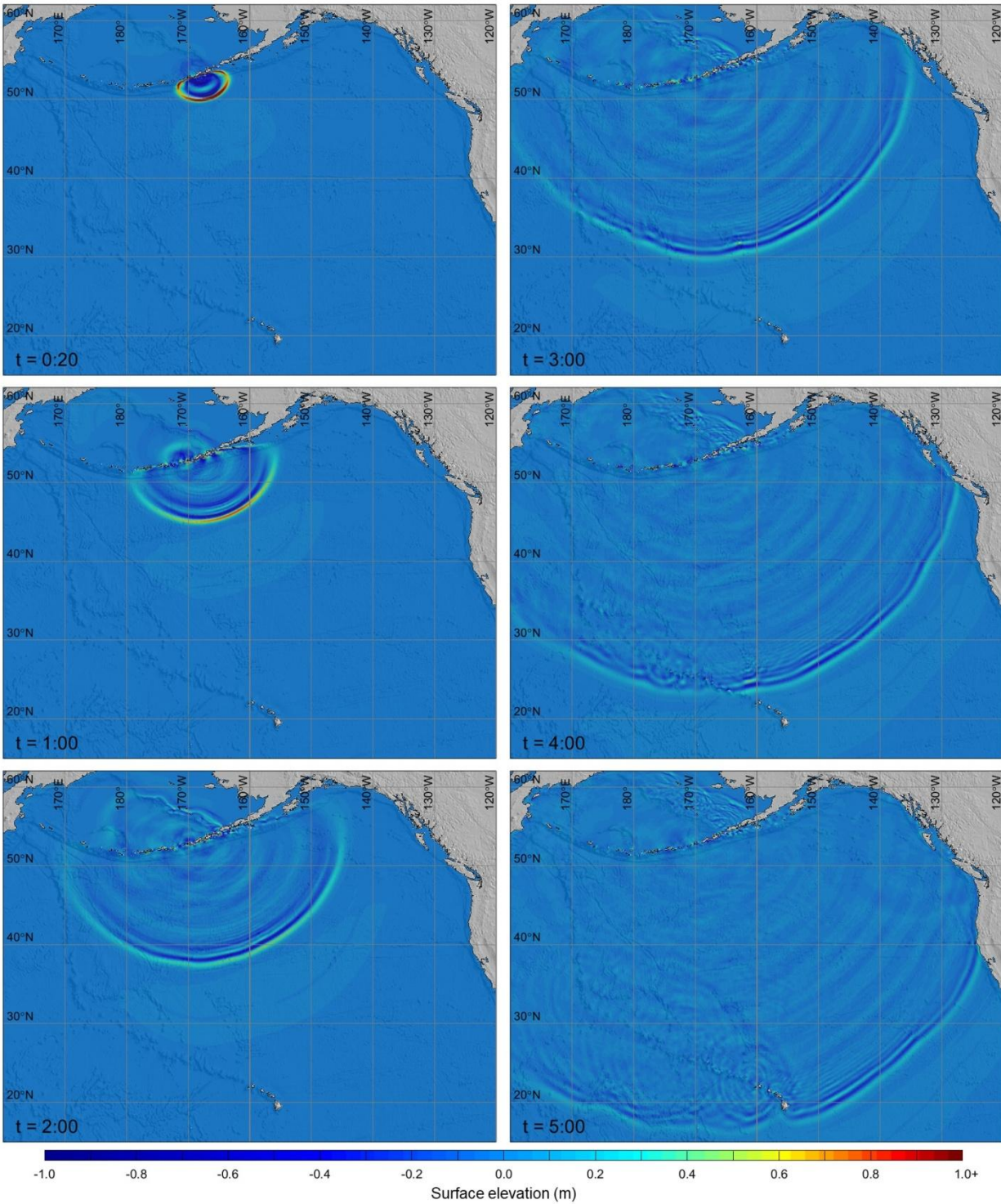
Supplementary Movies 1 to 3 (video files)

---

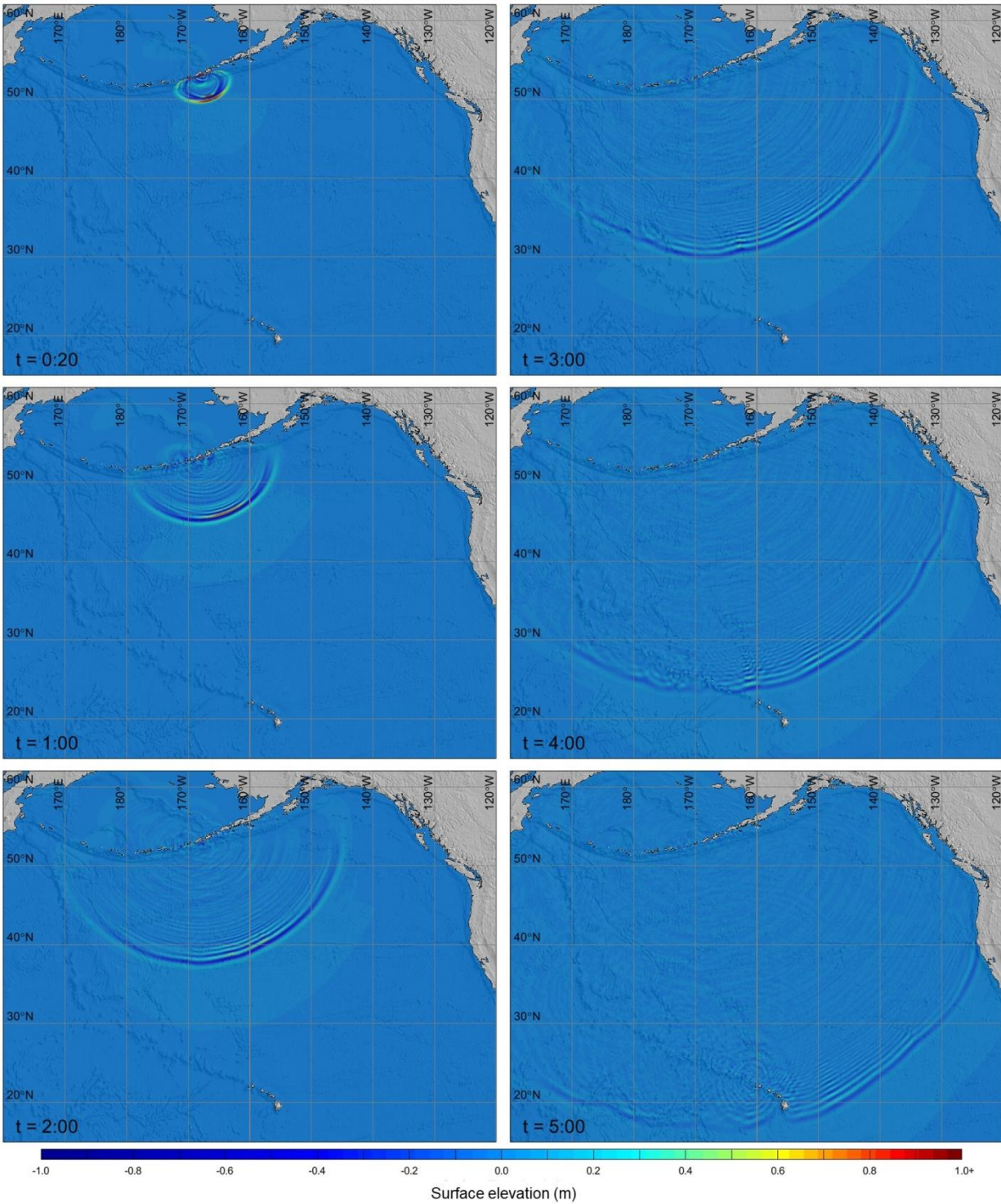
✉ email: [cheung@hawaii.edu](mailto:cheung@hawaii.edu)



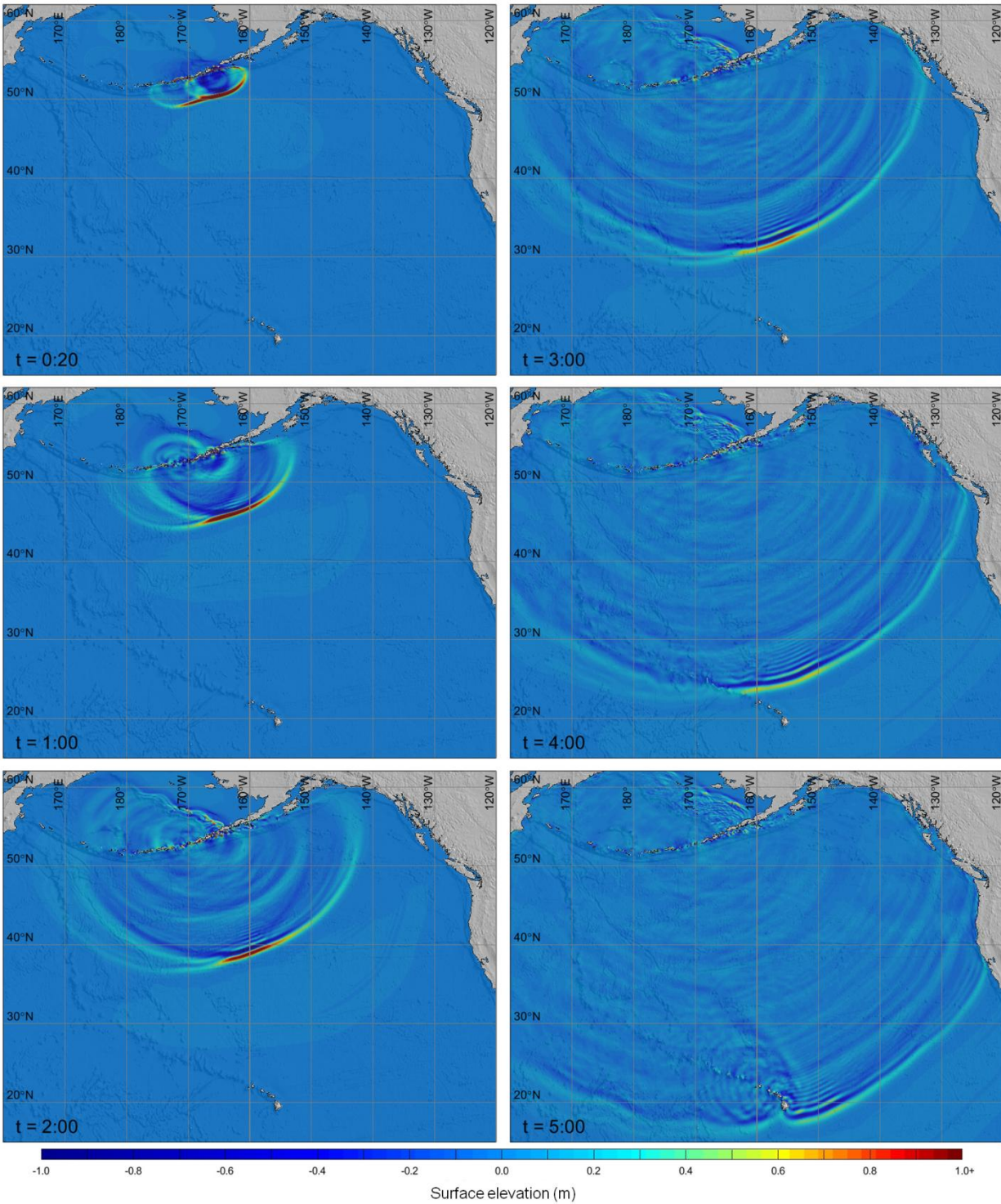
**Supplementary Fig. 1 | Layout of nested computational grids and locations of Stratigraphic records.** **a** Level-1 grid with level-2 eastern Aleutian and Hawaiian Islands grids denoted by rectangles. **b** Level-2 eastern Aleutian Islands grid with level-3 to 5 grids telescoping to the Driftwood and Stardust sites. **c** Level-2 Hawaiian Islands grid with level-3 to 5 grids telescoping to the Anahola, Kahana, and Pololū sites. Source data available from [https://www.gebco.net/data\\_and\\_products/gridded\\_bathymetry\\_data/](https://www.gebco.net/data_and_products/gridded_bathymetry_data/) and <https://www.ncei.noaa.gov/maps/bathymetry/>.



**Supplementary Movie 1 | Trans-Pacific tsunami propagation for the 18<sup>th</sup> century event.** Time  $t$  in Hr:Min after earthquake initiation and transparent water surface revealing bathymetric features. Base map generated from [https://www.gebco.net/data\\_and\\_products/gridded\\_bathymetry\\_data/](https://www.gebco.net/data_and_products/gridded_bathymetry_data/).



**Supplementary Movie 2 | Trans-Pacific tsunami propagation for the 15<sup>th</sup> century event.** Time  $t$  in Hr:Min after earthquake initiation and transparent water surface revealing bathymetric features. Base map generated from [https://www.gebco.net/data\\_and\\_products/gridded\\_bathymetry\\_data/](https://www.gebco.net/data_and_products/gridded_bathymetry_data/).



**Supplementary Movie 3 | Trans-Pacific tsunami propagation for the 14<sup>th</sup> century event.** Time  $t$  in Hr:Min after earthquake initiation and transparent water surface revealing bathymetric features. Base map generated from [https://www.gebco.net/data\\_and\\_products/gridded\\_bathymetry\\_data/](https://www.gebco.net/data_and_products/gridded_bathymetry_data/).